The Meteoritical Society

Meteoritics & Planetary Science 42, Nr 1, 93–112 (2007)
Abstract available online at http://meteoritics.org

Numerical modeling of impact-induced hydrothermal activity at the Chicxulub crater

Oleg ABRAMOV[†*] and David A. KRING[‡]

Lunar and Planetary Laboratory, 1629 East University Boulevard, The University of Arizona, Tucson, Arizona 85721–0092, USA
[†]Present address: Department of Space Studies, Southwest Research Institute, 1050 Walnut Street, Suite 400, Boulder, Colorado 80302, USA
[‡]Present address: Lunar and Planetary Institute, 3600 Bay Area Boulevard, Houston, Texas 77058, USA
[*]Corresponding author. E-mail: abramovo@boulder.swri.edu

(Received 22 February 2006; revision accepted 08 October 2006)

Abstract–Large impact events like the one that formed the Chicxulub crater deliver significant amounts of heat that subsequently drive hydrothermal activity. We report on numerical modeling of Chicxulub crater cooling with and without the presence of water. The model inputs are constrained by data from borehole samples and seismic, magnetic, and gravity surveys. Model results indicate that initial hydrothermal activity was concentrated beneath the annular trough as well as in the permeable breccias overlying the melt. As the system evolved, the melt gradually cooled and became permeable, shifting the bulk of the hydrothermal activity to the center of the crater. The temperatures and fluxes of fluid and vapor derived from the model are consistent with alteration patterns observed in the available borehole samples. The lifetime of the hydrothermal system ranges from 1.5 to 2.3 Myr depending on assumed permeability. The long lifetimes are due to conduction being the dominant mechanism of heat transport in most of the crater, and significant amounts of heat being delivered to the near-surface by hydrothermal upwellings. The long duration of the hydrothermal system at Chicxulub should have provided ample time for colonization by thermophiles and/or hyperthermophiles. Because habitable conditions should have persisted for longer time in the central regions of the crater than on the periphery, a search for prospective biomarkers is most likely to be fruitful in samples from that region.

INTRODUCTION

Impact-Induced Hydrothermal Systems

A hypervelocity impact of a large bolide into a planetary crust delivers a vast amount of energy, some of which is converted into heat. If water or ice is present in the crust, the resulting temperature increase provides a thermal driver for the circulation of water and the emission of steam, initiating a hydrothermal system. In particular, several long-term heat sources are created by a large impact event such as the one that formed the 65 Myr old and about 180 km in diameter Chicxulub crater: shock-deposited heat, a melt sheet, and a central uplift. In any hypervelocity impact, a shock wave compresses the target material, depositing large amounts of internal energy, and a subsequent decompression by rarefaction waves results in waste heat, which increases the temperature of the rocks (e.g., Ahrens and O'Keefe 1972). In large impacts, sufficient heat is deposited by the shock wave to induce phase changes and the melting and vaporization of target rocks. If enough impact melt is produced, it pools in the topographically lowest regions of the crater basin, forming a melt sheet. The final heat source is the central uplift, or material that has been uplifted from warmer regions of the crust during the crater formation process. The importance of the melt sheet and the central uplift relative to shock-emplaced heat increases with crater diameter. Small simple craters such as the Barringer meteorite crater (a.k.a. Meteor Crater) in Arizona produce negligible amounts of melt and uplift, while in large complex craters such as Chicxulub, the melt sheet and central uplift dominate the system. Melt sheets generally contribute significantly more energy than the heat from the uplifted geothermal distribution (Daubar and Kring 2001; Thorsos et al. 2001).

Mineralogical evidence of hydrothermal activity has been identified at a wide variety of terrestrial impact craters (Naumov 2002). Examples of mineralogical alteration range from craters as small as the 4 km Kärdla crater (Versh et al. 2005) to large impact basins such as Chicxulub (~180 km in diameter) (Kring and Boynton 1992; Ames et al. 2004; Hecht

et al. 2004; Zurcher and Kring 2004) and Sudbury (150 to 250 km in diameter) (Farrow and Watkinson 1992; Ames et al. 1998). Hydrothermal alteration is often found in the central uplifts (e.g., Naumov 2002), or, for large craters such as Chicxulub and Sudbury, in the permeable breccias on top of melt sheets (e.g., Ames et al. 1998). Hydrothermal alteration and mineralization have also been observed in the faulted crater periphery, impact-melt rocks, and postimpact sedimentary crater-fill deposits (see Osinski et al. 2005 for an overview).

Studies of terrestrial craters reveal three important features of impact-generated hydrothermal systems. First, the volume affected by hydrothermal activity is very large, often extending laterally across the entire diameter of a crater and to depths of several kilometers (e.g., Naumov 2002). Second, these systems have the capacity to significantly redistribute chemical elements and create chemical gradients throughout equally large volumes of the Earth's crust. Third, these systems have the same biogeochemical features as volcanically driven hydrothermal systems and, thus, may have influenced the biological evolution of Earth.

Impact events and any resulting hydrothermal activity may have been particularly important ~3.9–4.0 Gyr ago when the Earth and other inner solar system surfaces were severely bombarded (Turner et al. 1973; Tera et al. 1974; Ryder 1990; Cohen et al. 2000; Kring and Cohen 2002). During this inner solar system cataclysm, the heat delivered by impact events may have exceeded that generated by volcanic activity (Kring 2000). This cataclysm lasted from 20 to 200 Myr (e.g., Tera et al. 1974; Ryder 2000), virtually coinciding with the earliest possible evidence for life dating to 3.85 Gyr (Mojzsis and Harrison 2000). In addition, phylogenies constructed from rRNA sequences suggest that all terrestrial life has a thermophilic or a hyperthermophilic common ancestor (e.g., Pace 1997). This implies that perhaps the Earth's nascent biosphere was exterminated by the impact cataclysm, except for organisms that were able to adapt to hydrothermal conditions. Alternatively, these systems may have provided a site for life's origin. In either case, evidence suggests that impact events and the hydrothermal systems they initiated may have played an important role in the evolution of life on early Earth.

The overarching goal of this work is to quantify the significance of impact-induced hydrothermal systems through numerical modeling by focusing on their lifetimes, mechanics, and biological potential. The Chicxulub crater, located on the northern edge of the Yucatán Peninsula, provides an analogue of these ancient systems and can be used to constrain computer models of hydrothermal circulation with geological data. This crater has been extensively studied through the recent Chicxulub Scientific Drilling Project and analyses of previously collected samples, as well as extensive seismic, magnetic, and gravity surveys, allowing for the construction of a better-defined and better-constrained computer model. Starting conditions such as topography, permeability, and melt distribution are either very well known or can be adjusted to match rock-water ratios, temperatures, and degrees of alteration deduced from Chicxulub drill cores.

Chicxulub Crater

Of the three largest terrestrial impact craters (Vredefort, Sudbury, and Chicxulub), the 65 Myr old Chicxulub crater, linked to the K/T boundary mass extinction event, is by far the youngest and best preserved. Its original rim-to-rim diameter remains somewhat controversial, with estimates ranging from 130 to 300 km (see Kring 2005 for a review). A favored estimate of ~180 km (ranging from 170 to 200 km) is used in the model presented in this paper. The Chicxulub impact occurred into partially submerged Cretaceous sediments underlain by a crystalline silicate basement, and has since been buried by up to 1 km of Tertiary carbonate rocks (e.g., Kring 2005). Seismic data (e.g., Morgan et al. 1997, 2000) indicates the presence of a very pronounced peak ring, and less pronounced features that have been interpreted as outer ring structures in the periphery of the crater. Other structural characteristics detected at the Chicxulub crater are a central uplift, a central melt sheet, a far smaller amount of melt in the annular trough between the peak ring and the rim, and a modification zone in the same region, where blocks of Cretaceous sedimentary rocks slid down into the crater basin along a series of normal faults, forming tilted structural blocks. In addition to seismic, magnetic, and gravity surveys, the Chicxulub crater has been explored with drilling. Of the four drill holes inside the crater, three (Yucatán-6 [Y6], Chicxulub-1 [C1], and Sacapuc-1 [S1]) were oil prospecting boreholes, drilled by Petróleos Mexicanos. The fourth one, Yaxcopoil-1 (Yax-1), was a scientific borehole, drilled by the Chicxulub Scientific Drilling Project. The location of these boreholes and the main structural features of Chicxulub crater are shown in Fig. 1.

Hydrothermal Alteration at the Chicxulub Crater

The first evidence of hydrothermal activity at the Chicxulub crater, mainly in the form of anhydrite and quartz veins, was observed in the impact-melt rocks and overlying polymict impact breccias recovered from the Y6 borehole (Hildebrand et al. 1991; Kring and Boynton 1992; Schuraytz et al. 1994). A host of alteration products, including albitized plagioclase, secondary K-feldspar, quartz, epidote, chlorite, and pyrite and chalcopyrite traces, was subsequently identified in C1-N10, the only sample recovered from the central melt sheet (Schuraytz et al. 1994; Zurcher et al. 2005b). Unfortunately, the C1 and Y6 boreholes were not continuously cored and only provide fragmentary records.

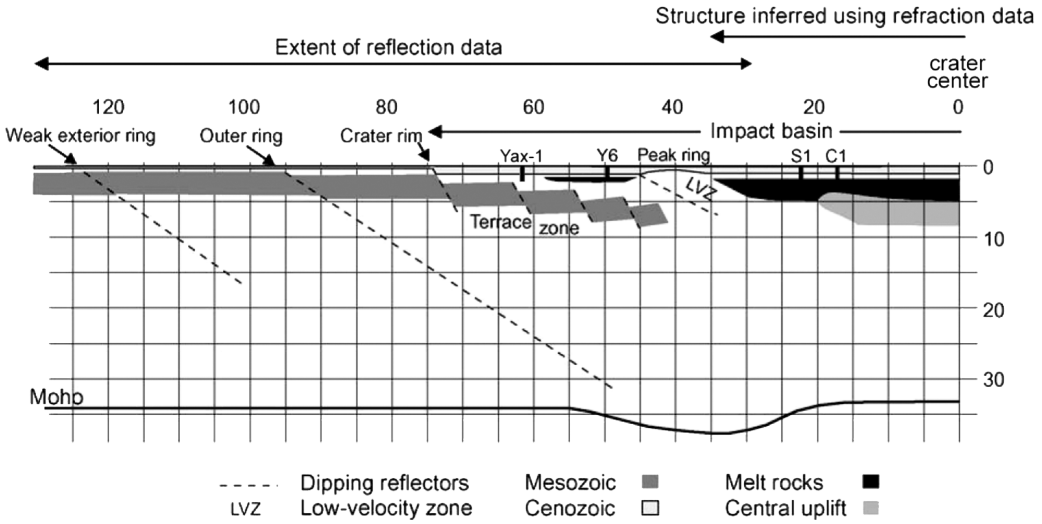

Fig. 1. A schematic cross section of the Chicxulub crater, derived mainly from seismic data, illustrating the major structural elements used in the model. Modified from Morgan et al. (2002).

Yaxcopoil-1, however, produced a continuous core throughout the impactite sequence and greatly expanded the spatial fidelity of hydrothermal activity at the crater. Petrographic, electron microprobe, and Raman spectrometry analyses of the impact melt and overlying breccias recovered from Yax-1 show unambiguous evidence of extensive hydrothermal alteration shortly after the impact (Zurcher and Kring 2004; Ames et al. 2004; Hecht et al. 2004), indicating that hydrothermal activity extended at least as far out as the annular trough.

Although hydrothermal activity clearly occurred, the peak temperature and the duration of peak temperature versus retrograde temperatures is more uncertain. Assemblages of diopside-hedenbergite (thermal metamorphic salitic pyroxene) after primary augite and widespread Na-K for Ca metasomatic alkali exchange (in the form of discrete veins with halos) suggest that, after an initial low-temperature phase, the temperatures in this hydrothermal system increased, perhaps to >300 °C (Zurcher and Kring 2004). Lower-temperature (<300 °C) alteration then followed in the form of diffuse K-feldspar replacement fronts, abundant calcite veins and open-space fillings, chlorite, and widespread smectite mainly after mafic minerals and clasts, as well as probable primary glass (Zurcher and Kring 2004). On the other hand, Ames et al. (2004) argue that the alteration mineral assemblages observed in samples from Yax-1 formed at relatively low temperatures (<150 °C). However, subsequent fluid inclusion (Lüders et al. 2003; Lüders and Rickers 2004) and isotopic studies (Zurcher et al. 2005a) show that hydrothermal fluid temperatures ranged from 100 °C (based on fluid inclusions in late calcite) to 270 °C (based on fluid inclusions in hydrothermal quartz veins).

The source of water for the hydrothermal system is also uncertain. Zurcher et al. (2005a) argue that, based on stable isotope results as well as mineralogical and compositional data, a basinal oil-field saline brine was in all probability the main source for the hydrothermal solutions. On the other hand, Ames et al. (2004) suggest the observed mineral assemblages point to a seawater incursion. The phase of the water that caused hydrothermal alteration at the Yax-1 site almost certainly included some vapor, as temperatures in excess of 250 °C would have been hard to achieve without boiling in this shallow environment (Zurcher et al. 2005a).

The amount of water that circulated through the impact breccias recovered from Yax-1 was modest but not necessarily dissimilar to that measured in other hydrothermal systems. Oxygen isotope data on silicate fractions estimate water/rock ratios of up to 2 for a closed system (Zurcher et al. 2005a), which is indicative of the minimum amount of water that migrated through the rock. These water/rock ratios imply that the Yax-1 site was not submerged at the time of hydrothermal activity. This is further supported by the lack of basal Tertiary foraminifera, suggesting that the Yax-1 site, which is about 300 m above the basin floor, was not submerged by foraminifera-bearing waters until at least about 300,000 yr after the impact (Kring, Forthcoming). Since it appears likely that the Yax-1 site was initially elevated above the water table and unsaturated, the observed water/rock ratios are not necessarily representative of the permeability in the rest of the system, which was submerged and saturated.

MODEL DESCRIPTION

Computer Code HYDROTHERM

For the work presented in this paper, we used a modified version of the publicly available program HYDROTHERM

(source code available from authors), a three-dimensional finite-difference computer code developed by the U.S. Geological Survey to simulate water and heat transport in a porous medium (Hayba and Ingebritsen 1994). The operating range of the program is 0–1200 °C and 0.5–1000 bars; however, the upper temperature limit has been extended by the authors to 1700 °C for the modeling of impact-melt sheets. A more detailed discussion of the theoretical basis of HYDROTHERM is presented in Abramov and Kring (2004) and references therein.

HYDROTHERM has previously been used to model a variety of hydrothermal systems; in particular, it was applied to the cooling of magmatic intrusions on Earth (e.g., Hayba and Ingebritsen 1997) and Mars (Gulick 2001), as well as hydrothermal systems at terrestrial (Abramov and Kring 2004) and Martian (Rathbun and Squyres 2002; Abramov and Kring 2005) impact craters.

Code Assumptions

Despite HYDROTHERM's general suitability for modeling impact-induced hydrothermal systems, there are several assumptions implicit to the code. First, the program assumes that the fluid is pure water, while hydrothermal fluids generally contain some other substances in solution. However, thermodynamic properties of terrestrial seawater at subcritical temperatures are sufficiently close to that of pure water for the purposes of this model, and the properties at supercritical temperatures are mostly irrelevant due to extremely low permeabilities (Hayba and Ingebritesen 1997). Another important assumption made by HYDROTHERM is local thermal equilibrium between the rock and water, which holds true if the fluid flow is relatively slow and steady, and breaks down for rapid transients. For this breakdown to occur, however, water would need to pass through 250 m of rock (the vertical resolution of our model) without reaching equilibrium, which is unlikely except perhaps in the very early stages of the system. A more important assumption made by HYDROTHERM is that the ground remains fully saturated throughout the simulation, meaning that all pore spaces remain filled by water, steam, or a combination of the two. In our models, the surface of the water filling the crater represents the level of the groundwater table, and the ground below that datum is expected to be fully saturated. The permeability and porosity of the rocks above that datum are set to near-zero to approximately simulate an unsaturated elevated surface. The reasons for this are: i) the flux through the rim due to atmospheric precipitation is insignificant compared to the fluxes in an active hydrothermal system; ii) without knowing the exact geometry of the crater and surface properties, it is impossible to predict how much of the rainfall would seep into the ground and how much of it would drain into the crater basin; and iii) the temperatures in the rim region are essentially ambient, and any water flow through it would not affect the thermal evolution of the crater. This "dry" approximation is not perfect because some water flow can occur in the unsaturated zone through mechanisms such as capillary action, but only small regions of the crater, most notably the upper portion of the peak ring, are affected. While the water table beyond the crater rim may be higher, it would not significantly affect hydrothermal circulation due to the relatively low temperatures in that area.

Model Resolution and Boundary Conditions

Taking advantage of an impact crater's radial symmetry, we examine a vertical cross section from the center of the Chicxulub crater to beyond its outer rim. The model is represented on a 150 × 66 grid with a total of 9900 blocks, corresponding to a horizontal resolution of 1 km and vertical resolution of 250 m. The model's upper boundary represents a thin layer of cooled breccia, with pressure and temperature held constant at 1 atm and 25 °C. The thickness of this breccia layer is equal to the model's vertical resolution of 250 m. It functions as an infinite source or sink of the fluid, donating or accepting water depending on underlying hydrologic conditions, except in cases where it is located above the water table. It also functions as a heat sink; so when the thermal energy reaches the upper boundary, it is permanently removed from the system to simulate heat loss to the water filling the crater and eventually to the atmosphere. The bottom boundary is impermeable and subjected to a constant basal heat flux of 32.2 mW/m^2 to match a geothermal gradient of 13 °C km^{-1} (as described further below). The left boundary of the model is the crater's axis of symmetry and is therefore impermeable and insulating. The right boundary is permeable for both fluid and heat. It is located sufficiently far away from the point of impact that the temperatures are close to an average geothermal gradient.

INPUT PARAMETERS

Topography

Because the Chicxulub crater is buried under a thick layer of Tertiary sediments, seismic sounding provides the best means of determining its original topography (although several boreholes have been drilled, they are not yet sufficient to define many details of the topography). Seismic reflection data indicates that the peak ring has an average radius of 40 km, measured to the highest point (e.g., Morgan et al. 1997), and a lateral thickness of ~10 km (e.g., Morgan et al. 2002). The height of the peak ring observed in the seismic reflection data is up to 600 m above the crater floor (e.g., Morgan et al. 1997), but the model peak ring height was rounded up to 750 m to take probable erosion into account. The depth of the crater below the pre-impact surface has been estimated to be 860 m, and the height of the rim at 540 m, by

Bell et al. (2004) based on the scaling laws of Grieve and Pesonen (1992) and Pike (1977). Due to the resolution of the model, these numbers were rounded to 750 m for crater depth and 500 m for rim height.

Temperature Distribution

The shock-deposited energy attenuates rapidly from the point of impact in a predictable way (e.g., Robertson and Grieve 1977), but large quantities of material are subsequently displaced and relocated during the modification phase of crater formation, making analytical estimation of temperature fields very difficult. Therefore, hydrocodes are usually used to generate postimpact temperature distributions. The temperature distribution used in this model was generated with a SALEB hydrocode calculation specifically for the Chicxulub crater by Boris A. Ivanov (personal communication). This temperature distribution is an updated version, slightly different from that described in Ivanov (2004). The impactor was modeled as an ANEOS granite asteroid 14 km in diameter impacting at a velocity of 12 km/s. Although it is still unclear if the Chicxulub crater was produced by an asteroid or a comet, as appropriate transient crater diameters can be produced by both types of objects (Pierazzo et al. 1998), the Ivanov (2004) model produces a final crater diameter of ~180 km, which is consistent with geophysical imaging of the subsurface structure.

The geothermal gradient in the model by Ivanov (2004) is rather low (13 °C/km) compared to heat flows of 65–80 mW/m^2 (and implied gradients in the crust of 26 to 32 °C km) observed at Chicxulub by Wilhelm et al. (2004). Therefore it should be treated as conservative temperature estimate, possibly leading to an underestimation of the duration of hydrothermal activity.

While the climate of the mid-Cretaceous was significantly warmer than today—with estimated global mean temperatures about 6 to 12 °C higher than in the present (e.g., Barron 1983)—toward the end of Cretaceous Period the temperatures cooled by as much as 8 to 10 °C. This is supported by several lines of evidence, including oxygen isotopes and foliar physiognomy (e.g., Frakes 1979). Estimates of average equatorial sea surface temperatures in the late Cretaceous generally fall between 20 and 30 °C (e.g., Huber et al. 1995; Kolodny and Raab 1988). The estimates of average tropical air temperatures during that time period fall within the same range (e.g., Upchurch and Wolfe 1987). Therefore we use a surface temperature of 25 °C in our model.

Melt Properties

Central Melt Sheet

The SALEB hydrocode model by Ivanov (2004) does not explicitly include a near-surface melt sheet, but it was incorporated into our model based on observed data. Three-dimensional seismic tomography suggests that the Chicxulub central melt sheet has a maximum thickness of 3.5 km in the center of the crater (Morgan et al. 2000). This approximation is also supported by the gravity modeling of Ebbing et al. (2001), who estimate a central melt thickness of ~3 km, which is consistent with previous scaling approximations (Kring 1995). However, Christeson et al. (2001) interpret the seismic and gravity data as suggestive of a melt sheet that is only 1 km thick. The model presented in this paper assumes a melt sheet with a central thickness of 3 km and thinning radially. This is consistent with the Pope et al. (2004) estimate of a 3.5 km central melt sheet at Chicxulub (with the caveat that the bottom 2.5 km may be a "melt breccia" that is only 65% melt) based on crater geometry and lithological data from boreholes.

The lateral extent of the central melt sheet is not as well defined. Pilkington et al. (1994) and Ebbing et al. (2001) suggested that the central melt body has a radius of 45 km based on gravity and magnetic data, implying a continuous melt sheet beneath the peak ring, the highest point of which has a radius of ~40 km. However, analysis of seismic data by Morgan et al. (2000, 2002) indicates that there is a zone of lowered velocity directly beneath the topographic peak ring, with velocities too low to represent pure melt rocks. It was therefore suggested that the melt sheet terminates at the inner edge of the peak ring, and a separate melt sheet is present in the annular trough between the peak ring and the crater rim (Fig. 1). This is consistent with several boreholes drilled on either side of the peak ring (e.g., Fig. 8 of Kring et al. 2004).

Impact melt is initially superheated (e.g., Hörz 1965; El Goresy 1965; Carstens 1975; Grieve et al. 1977) to temperatures as high as 2200 °C (and possibly higher), but the effective starting temperature of an impact-melt sheet is highly dependent on the volume proportion of cold clasts incorporated into it (e.g., Onorato et al. 1978). This proportion is not well established for Chicxulub, as the only sample from the central melt sheet (C1-N10) does not contain any relict target clasts (e.g., Sharpton et al. 1992). However, it can be assumed the proportion of clasts in the melt decreases with the increasing size of the impact event (e.g., Prevec and Cawthorn 2002) because larger transient craters have a higher proportion of melt with respect to excavation volume (O'Keefe and Ahrens 1977). For large impact craters like Sudbury (Prevec and Cawthorn 2002) and Chicxulub, the proportion of clasts in the melt may have been lower than in smaller craters like the ~100 km in diameter Manicoagan crater (Onorato et al. 1978). Therefore, the initial temperature of the central melt sheet in our model is conservatively estimated to have been 1700 °C, allowing for at least 500 °C of cooling due to the initial thermal equilibration between superheated melt and entrained cold clasts. At Chicxulub, this initial estimate is supported by peak temperature of melt fragments in the

suevitic units recovered from the Yax-1 drillcore, which exceeded 1700 °C based on the decomposition of zircon (Wittmann et al. 2005). Also, the melt in the impact-melt dikes observed in the Yax-1 borehole quickly impregnated a dolomitic host rock, suggesting a low viscosity and, thus, high initial temperatures (Wittmann et al. 2004). The initial temperature of the model's central melt sheet is uniform, as petrologic studies of impact-melt-derived rocks at a variety of terrestrial impact craters show that clasts of diverse provenance tend to be evenly mixed throughout the sheet, probably due to turbulent mixing during melt aggregation (Phinney and Simonds 1977). Although melt sheet margins are rapidly cooled during the final stages of crater formation, as indicated by an abundance of undigested clasts within a few meters of the basal contact (e.g., Simonds et al. 1976), the temperature of the interior is expected to be largely homogeneous as a result of this turbulent mixing. Postimpact convection in the central melt sheet is unlikely to have significantly contributed to the cooling of the melt due to substantial viscous damping in systems like Chicxulub that occur in siliceous continental crust (Onorato et al. 1978; Kring 1995), and is not modeled here.

Melt in the Annular Trough

It is not clear whether the melt in the annular trough forms a continuous layer between the peak ring and the outer wall or whether there are discontinuous melt pools in the crater's modification zone (Kring 2005). For the purposes of this paper, we assume a continuous pool between the radii of 45 and 58 km as suggested by Morgan et al. (2002) based on seismic data (Fig. 1). The depth of the melt in the model annular trough ranges from 250 to 500 m, based the thickness of the melt unit in the Y6 borehole (380 m), which bottomed in 6 to 8 m of anhydrite. This might be a conservative estimate because the anhydrite may be a large clast within the melt unit, in which case the melt thickness in Y6 is greater than 380 m (Kring et al. 2004). The melt is underlain by Cretaceous sediments, based on a tentative detection in Y6 and a definite detection in Yax-1. The melt thins radially until its thickness is below the resolution of the model, so it is zero at the position of the Yax-1 borehole, where the actual melt thickness is ~24–34 meters.

The initial temperature of melt in the annular trough was probably lower than that of the central melt sheet. There are indications of rapid cooling, likely due to a high clast content and relatively cooler bounding lithologies. For example, a melt sample from the annular trough (Y6-N17) has smaller crystals than a melt sample from the central melt sheet (C1-N10), suggesting faster cooling (Schuraytz et al. 1994; Kring 1995). Also, melt rocks from the Yax-1 borehole appear to have been quenched to below 600 °C fast enough for relict zircons to survive (Wittmann et al. 2005). It should be noted, however, that the melt sampled in Yax-1 is either from the extreme outer edge of the melt sheet in the annular trough or from a small and shallow melt pool, so its initial temperature is expected to be significantly lower than that in the central portion of the annular melt sheet. Finally, a sample (Y6-N17) from a thicker portion of the impact melt was found to contain undigested clast abundances from 2% (Kring and Boynton 1992) to 35% (Schuraytz et al. 1994), with at least 44% of the initial clast volume digested (Kring 1995). This indicates that melt in the annular trough was initially at a high temperature, but dipped below the liquidus through thermal equilibration before all clasts were fully digested. Therefore, the temperature of this melt was set to 1087 °C, a midpoint between the liquidus and solidus temperatures.

Physical Parameters of the Melt

The total volume of melt in the central melt sheet and the annular trough of the model crater is estimated to be 12,000 km^3, which is almost identical to the 12,631 km^3 proposed by Pope et al. (2004). As described in the previous sections, this number is generated from constraints imposed by crater geometry, seismic, gravity, and magnetic data, and four boreholes. This estimate does not include melt in overlying breccias, melt in dikes, and melt ejected out of the crater, so the total melt generated by the impact was significantly higher. For example, the breccias recovered from the Yax-1 borehole are composed of up to 85% melt fragments (Kring et al. 2004) and ~25% of the total melt was previously estimated to have been ejected (Kring 1995).

The latent heat of fusion is included in the model using the approximation of Jaeger (1968), as used by Onorato et al. (1978) in a study of the Manicouagan impact-melt sheet, replacing the heat capacity C_p in the temperature range between the liquidus (T_L) and the solidus (T_S) with

$$C_p' = C_p + L/(T_L - T_S) \quad (1)$$

Here, L is the latent heat of fusion of diopside (421 kJ kg^{-1}). The liquidus and solidus temperatures of 1450 K (1177 °C) and 1270 K (997 °C), respectively, have been estimated by Ariskin et al. (1999) for the melt sheet of the Sudbury crater, which also formed on a continental crust and has a composition similar to that of Chicxulub (Kring 1995). The liquidus temperature agrees well with the value of 1150 °C estimated for the Chicxulub melt sheet by Warren et al. (1996) using the MELTS computer program.

Rock Properties

General Physical Parameters

In our model, rock porosity decays exponentially with depth to account for the pore space closing by lithostatic pressure, following the approach suggested by Binder and Lange (1980) for the lunar crust:

$$\Phi(z) = \Phi_0 \exp(-z/K) \quad (2)$$

The decay constant K scales with gravity to 1.07 km for

Earth (Clifford 1993), and the depth z is measured with respect to local topography, not the pre-impact surface level. Mayr et al. (2005) estimated that the porosity of polymict breccias recovered from the Yax-1 borehole averages about 0.25, which we use as the surface porosity value (Φ_0) in the model. Although porosity has been directly measured in boreholes at several impact craters, including Chicxulub, it has been extensively affected by postimpact processes such as hydrothermal and diagenetic mineralization, compaction, sedimentation, lithification, and tectonic activity. We therefore use lunar estimates (scaled for Earth) because they represent a pristine state immediately after the impact.

The fracture density underneath an impact crater is expected to decrease with depth (e.g., Nordyke 1964) and, thus, permeability in our model decreases exponentially with depth in the same way as porosity. The rate at which permeability decreases with depth is similar to that described by Manning and Ingebritsen (1999) based on geothermal data and metamorphic systems. Permeability is also a function of temperature, due to the brittle/ductile transition at about 360 °C in silicic rocks (Fournier 1991). This effect is modeled by log linearly decreasing permeability between 360 and 500 °C, following the approach of Hayba and Ingebritesen (1997):

$$k(z) = k_0 \exp(-z/K) \qquad T < 360\ ^\circ\mathrm{C} \qquad (3)$$

$$\log k(z, T) = \frac{\log k(z, T) + 11}{500 - 360}(500 - T) - 11 \qquad 360 \le T \le 500\ ^\circ\mathrm{C}$$

$$k = 10^{-11}\ \text{darcies} \qquad T > 500\ ^\circ\mathrm{C}$$

Partly based on the degree of alteration and the modest water/rock ratios estimated for the Yax-1 samples (Zurcher et al. 2005a), the surface permeability k_0 used in this model is 10^{-3} darcies, which is an order of magnitude smaller than the surface permeability used in our previous model for Sudbury crater (Abramov and Kring 2004). This is consistent with the estimate of Mayr et al. (2005), who measured permeabilities ranging from 10^{-2} darcies to 10^{-9} darcies in present-day rocks recovered from Yax-1, with the caveat that in situ permeability must be dominated by macroscopic fractures. We use a baseline postimpact permeability that is generally higher than present-day permeability estimates to take into account permeability decrease over time due to compaction and mineral precipitation. Also, large-scale, in situ postimpact permeability is likely dominated by macroscopic fractures not measured in the lab. Permeability has important effects on the dynamics and duration of a hydrothermal system, and is one of the most difficult variables to constrain in the model. Therefore, the effects of surface permeabilities an order of magnitude smaller and larger than 10^{-3} darcies were also investigated in this study. In addition, zones of doubled permeability, extending to a depth of 6 km, with a thickness of two model cells (2 km), and a dip of 45°, were introduced to simulate faults in the crater's modification zone. Due to model resolution, these faults were incorporated as overlapping 1 km vertical segments.

The relationship described in Equation 3 implies that an impact-melt sheet will become permeable as it cools below the brittle/ductile transition. This is consistent with observations that both the central melt sheet and the melt in the annular trough were sufficiently fractured to allow hydrothermal circulation though them. For example, as previously described, C1-N10, the only sample recovered from the central melt sheet, contains a host of alteration products (Schuraytz et al. 1994; Zurcher et al. 2005b), and melt rocks recovered from the Y6 and Yax-1 boreholes, which sampled the annular trough, are also significantly altered. The mechanisms that cause melt sheets to fracture may include thermal stresses from cooling and postimpact tectonic activity.

Physical Parameters of Cretaceous Sedimentary Rocks

Before the Chicxulub impact, Cretaceous sediments formed a sedimentary sequence 3 km thick overlying the crystalline basement. During the impact, almost all sediments that were within the transient crater (roughly within the peak ring) were vaporized or ejected out of the crater. This is supported by both seismic data (e.g., Morgan et al. 1997) and hydrocode modeling (Ivanov 2004). The sedimentary layers outside of the peak ring, on the other hand, remained relatively intact but collapsed into the crater during the modification stage, forming a terrace zone illustrated in Fig. 1.

The Cretaceous sedimentary succession includes limestone, dolomite, marl, and anhydrite. For the purposes of this model, pure limestone sediments were assumed, and their physical properties are summarized in Table 1. The physical properties used are those of Cretaceous limestones recovered from Yax-1 (Mayr et al. 2005), as well as Tertiary limestones from the same borehole (Popov et al. 2004), which have been more thoroughly analyzed at the time of writing.

While the thermal conductivity of sediments is often less than that of crystalline rocks, the thermal conductivity of Cretaceous sediments in the model is set to the same value as that of basement rocks (2.5 W m^{-1} K^{-1}), for consistency with the hydrocode model of Ivanov (2004), which generated the initial temperature distribution used here. This also agrees with the average value for limestone of 2.56 W m^{-1} K^{-1} from Clark (1966), and physical measurements on limestones from the Yax-1 borehole (Mayr et al. 2005), which give an average value of ~2.5 W m^{-1} K^{-1}.

Physical Parameters of Basement Rocks

Chicxulub basement rocks were originally covered by 3 km of sediments, but the impact delivered them to the surface (in both solid and liquid state) in the region within the peak ring (e.g., Morgan et al. 2000; Collins et al. 2002; Ivanov 2004). Crystalline clasts found in impact breccias suggest that

Table 1. Rock parameters used in the model.

Parameter	Value	Units
Porosity	f(z), 25% at the surface	Unitless
Permeability	f(z,T), 10^{-3} at the surface[a]	darcies
Thermal conductivity (basement, melt, breccia)	2.5	W m^{-1} K^{-1}
Heat capacity (basement, melt, breccia)	1000	J kg^{-1} K^{-1}
Density (basement, melt, breccia)	2700	kg m^{-3}
Thermal conductivity (sediments)	2.5	W m^{-1} K^{-1}
Heat capacity (sediments)	730	J kg^{-1} K^{-1}
Density (sediments)	2300	kg m^{-3}

[a]Unless otherwise indicated.

the basement is composed of a wide spectrum of lithologies, including granites, granitic gneisses, quartzites, quartz-mica schists, and amphibolites (Kring et al. 1991; Hildebrand et al. 1991; Kring and Boynton 1992; Sharpton et al. 1992, 1996; Kettrup and Deutsch 2003). Physical properties (density, thermal conductivity, and heat capacity) typical of the continental crust are used to represent these diverse lithologies and are summarized in Table 1. Also, the physical properties of the melt are assumed to be the same, because the melt is derived primarily from the basement rocks (e.g., Kring and Boynton 1992; Pierazzo et al. 1998).

Physical Parameters of Breccias

Polymict impact breccias rich in impact-melt fragments (suevites) have been observed directly above the impact melt in all drillcores within the final crater rim. The thickness of these suevites ranges from ~450 m in the S1 borehole (Hildebrand et al. 1991) above the central melt sheet to ~66 m in the Yax-1 borehole (Dressler et al. 2003) in the modification zone. The breccia thickness in the model ranges from 250 to 500 m, with the greatest thickness over the central melt sheet and in the region of the peak ring, to account for the zone of low seismic velocity observed there by Morgan et al. (2000, 2002). The suevites are composed primarily of melt fragments and crystalline clasts (e.g., Kring et al. 2004; Stöffler et al. 2004), hence their physical properties have been set identical to those of impact melt and crystalline basement. The polymict breccias at Chicxulub appear to have been deposited at relatively low temperatures of no more than a few hundred degrees C (or very quickly quenched to these temperatures), because the carbonate-rich matrix did not form a carbonatite-like melt, and micritic carbonate clasts in the carbonate-rich matrix were not resorbed (Kring et al. 2004). Several excavation, transportation, and depositional processes were likely involved. This contrasts with the fallout suevites at the ~25 km Ries crater, which appear to have been deposited at much higher temperatures of at least 680–750 °C (Engelhardt et al. 1995), or even higher (Osinski et al. 2004). The initial temperature of the breccias in the model was set to 250 °C, as a conservative estimate based on observations at Chicxulub.

Beyond the final crater rim there are two other types of polymict breccias, one being similar to the Ries fallout suevite and the other being similar to the Ries Bunte breccia (e.g., Kring 2005). Based on previous modeling experience (Abramov and Kring 2004; Abramov and Kring 2005), these were not included in the current model because they were unlikely to have significantly affected hydrothermal circulation.

RESULTS

Hydrothermal System Mechanics and Duration

The overall setup of the model is illustrated in Fig. 2, showing the temperature distribution immediately after the impact, major features of the model, and the area of interest. Almost all hydrothermal activity in the model occurs in the area within the dashed rectangle, and all subsequent figures focus on this area.

The baseline simulation of hydrothermal activity at the Chicxulub crater is presented in Fig. 3. The first timestep is at 4000 yr (Fig. 3a), where some thermal changes can already be observed, compared to the temperature distribution immediately after crater formation (Fig. 2). The melt in the annular trough, for instance, has long reached its solidus temperature, but is still sufficiently warm to be impermeable to fluids. This melt has completely crystallized in only ~600 yr, but the outlying regions would have crystallized much quicker, which is consistent with fine crystals observed in the Y6-N17 sample from near the top of the melt. Some cooling can be observed in the central melt sheet, too, and, although some of its peripheral regions have crystallized, the bulk still remains well above the liquidus. The thermal energy of the central melt sheet raised the temperature of a small portion of the central uplift above 1200 °C, suggesting some melting in that region after the impact. In terms of fluid circulation, there is significant circulation through the breccias above the central melt sheet. By this time, partial flooding of the deepest portions of the crater cavity by groundwater and/or seawater likely occurred (e.g., Goto et al. 2004). This water quickly infiltrated the permeable breccias over the melt, resulting in a short-lived period of intense steam generation within the breccias lasting ~2000 yr (not shown), followed by the circulation of water through these

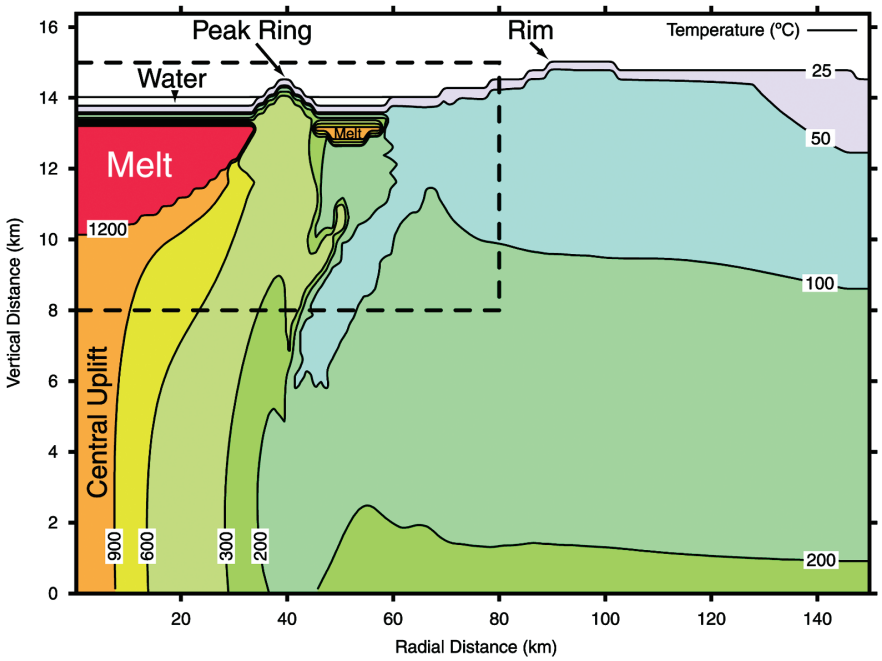

Fig. 2. Overall model geometry, based on a variety of constraints, and initial temperature distribution immediately after the impact, based on work by Ivanov (2004). Major structural features are indicated. Subsequent figures are limited to the area of interest inside the dashed rectangle.

breccias as seen in this timestep. The downward flow of water is not shown in Fig. 3a, because the permeable breccia layer is only one cell thick and immediately below the upper boundary, which automatically donates the replacement fluid. A large amount of steam is being generated beneath the peak ring, mostly originating near the critical point of water (374 °C). Convection cells have formed on either side of the peak ring and at the far side of the melt in the annular trough, with some water flow underneath the melt toward the peak ring.

At 20,000 yr (Fig. 3b), the system is significantly cooler and circulation is a bit weaker, with maximum fluxes about a factor of 2 smaller than those seen at 4000 yr. There are noticeable deflections in the temperature contours due to the upward flow of warmer water and downward flow of colder water. The central melt sheet has cooled significantly but still remains partly molten, and water continues to circulate through the permeable breccias above it. Some steam is beginning to be produced as the upper portion of the melt sheet is beginning to become permeable to fluids. The two convection cells on either side of the peak ring are still active, and some steam continues to be generated below the peak ring, albeit at a significantly reduced rate and generally at a greater depth. The melt in the annular trough has completely cooled and is now permeable to water, and the region is now a site of a convection cell with significant fluxes. On the far right of Fig. 3b, minor amounts of groundwater can be seen flowing toward the crater and moving up in the vicinity of one of the faults in the crater's modification zone, driven by the increased temperatures in the area.

By 200,000 yr (Fig. 3c), the central melt sheet has fully crystallized. Most of the hydrothermal activity in this timestep takes place above the central uplift, where numerous convection cells have formed. The water flux magnitudes are similar to those observed at 20,000 yr. A significant amount of steam is being generated over the central uplift. There is a significant upwelling below the peak ring, fed by a downwelling in the annular trough. Groundwater continues to seep upward near a fault in the modification zone.

Finally, at 2 million years (Fig. 3d), water flux magnitudes have decreased by a factor of about 20 from the previous timestep. The central uplift has cooled and is now fully permeable, driving a large central convection cell. There is still a long-lived upwelling below the peak ring. Given the low volumes of circulating water and the distances they must pass through, water probably cooled off almost completely before reaching the surface. It should also be noted that these fluxes may be smaller or nonexistent due to the closing of fractures by mineralization and clay deposition, processes that can clog hydrothermal systems over long periods of time (see the Discussion section). Figure 3d also provides a good overview of the circulation patterns in the crater's modification zone present but not immediately apparent in Figs. 3a–c. Note a downward water flow along a fault at a radius of ~77 km, as well as an upward flow in the region of a fault at ~69 km, indicated by a grey arrow and also seen in Figs. 3b and 3c.

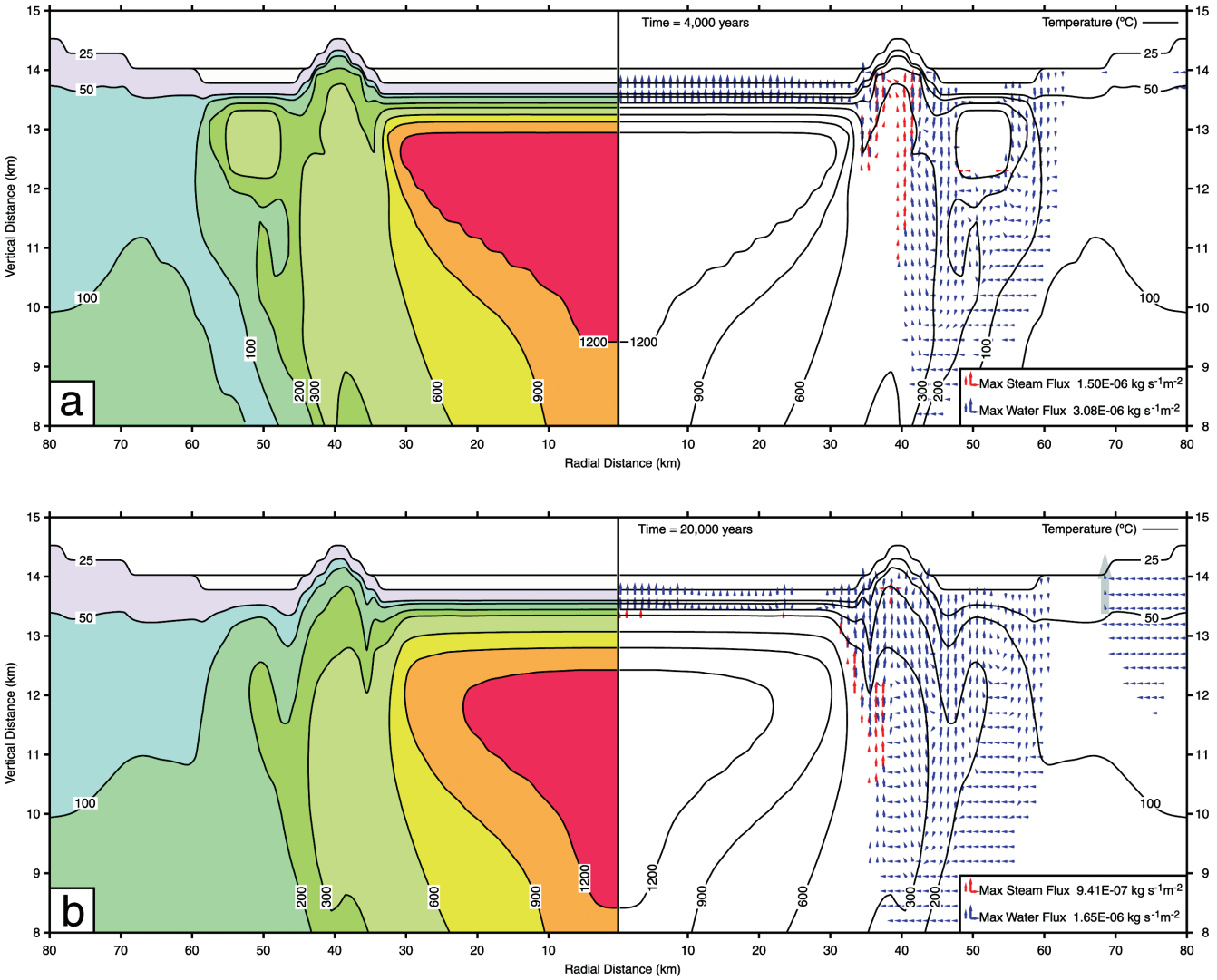

Fig. 3. Results of a numerical simulation of the hydrothermal system at Chicxulub crater. Surface permeability k_0 is 10^{-3} darcies. Black lines are isotherms, labeled in degrees Celsius, and blue and red arrows represent water and steam flux vectors, respectively. The lack of arrows indicates that fluxes are at least 2 orders of magnitude smaller than the maximum flux. The length of the arrows scales logarithmically with the flux magnitude, and the maximum value of the flux changes with each plot. Large gray arrows indicate upward water flow through a fault zone in the crater's modification zone.

Borehole Model Temperatures

The model allows tracking of temperatures at the locations of boreholes, permitting a comparison of temperatures and thermal histories to those inferred from the samples. Figures 4a–c show the temperature history of the upper 250 m of impact melt sampled by the C1, S1, and Y6 boreholes. For comparison, melt sample C1-N10 was recovered ~140 m below the top of the melt sheet, and samples Y6-17 and Y6-N19 were recovered ~50 and ~130 m, respectively, below the top of the melt. The model melt in C1 and S1 starts out at an initial temperature of 1700 °C and reaches the liquidus, represented by the first kink in the curve, at ~1000 yr, and the solidus, represented by the second kink in the curve, at ~3500 yr. In both cases, the melt cools to 500 °C by ~25,000 yr, with the C1 melt cooling slightly slower due to its location closer to the center of the melt sheet. The melt in Y6, which is in the annular trough, starts out at 1087 °C, reaches the solidus in ~500 yr and drops to 500 °C in ~3000 yr.

The melt unit in Yax-1 is only ~24–34 m thick and thus below the resolution of the model. To correct for this, a simple heat conduction model of the nearby region was constructed (further described in the Discussion section and schematically illustrated in Fig. 8a). Figure 4d shows the temperature history of the center of the 24 m thick melt unit in Yax-1 derived from this local model. The melt in Yax-1 cools quickly from an initial temperature of 760 °C, reaching 500 °C in ~5 yr and 50 °C in ~500 yr.

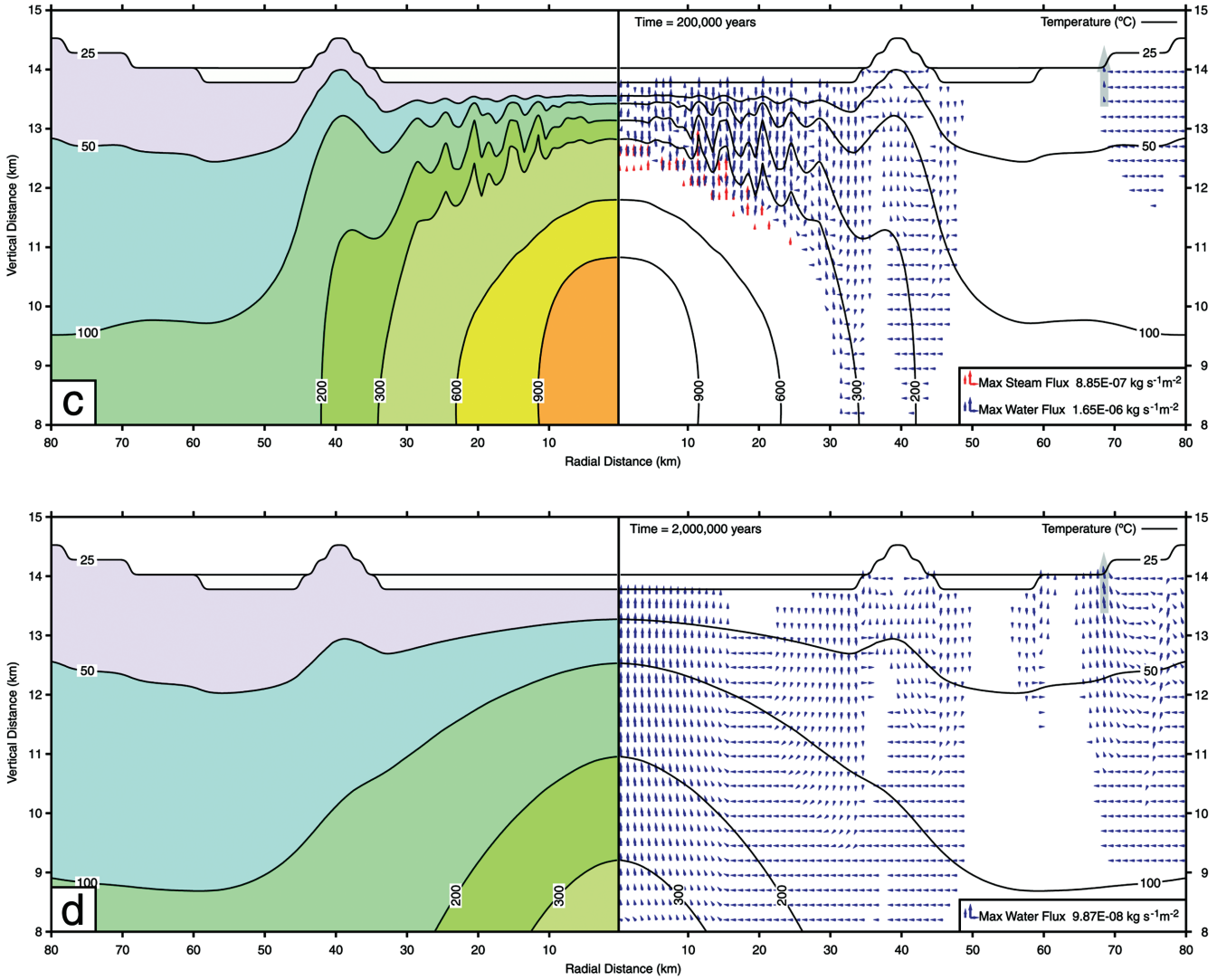

Fig. 3. *Continued.* Results of a numerical simulation of the hydrothermal system at Chicxulub crater. Surface permeability k_0 is 10^{-3} darcies. Black lines are isotherms, labeled in degrees Celsius, and blue and red arrows represent water and steam flux vectors, respectively. The lack of arrows indicates that fluxes are at least 2 orders of magnitude smaller than the maximum flux. The length of the arrows scales logarithmically with the flux magnitude, and the maximum value of the flux changes with each plot. Large gray arrows indicate upward water flow through a fault zone in the crater's modification zone.

Effects of Permeability

Higher-Permeability Case

Figure 5 shows the evolution of the hydrothermal system with the surface permeability k_0 set an order of magnitude higher, or to 10^{-2} darcies. While the overall system dynamics are generally similar, there are several differences that are immediately apparent: water and steam fluxes are about a factor of 10 higher, temperature contours are more strongly deflected by upwellings and downwellings, and the system cools more rapidly. At 4000 yr, the convection cells on both sides of the peak ring have a greater vertical extent. At 20,000 yr, the top 250 m of the central melt sheet has cooled a little quicker, and is being permeated by water. There are also more convection cells in the annular trough region. Another obvious difference is at the 200,000 year timestep, where the convection cells above the central uplift are significantly higher in number and larger in the vertical dimension. Also, the temperatures beneath the peak ring are considerably lower. At the 2,000,000 year timestep, the system is significantly cooler: the 300 °C contour is entirely absent. An additional dissimilarity here is the presence of three convection cells in the central region of the crater, as opposed to a single central upwelling.

Lower-Permeability Case

The circulation patterns in the model with a surface permeability k_0 of 10^{-4} darcies (not shown) are similar to

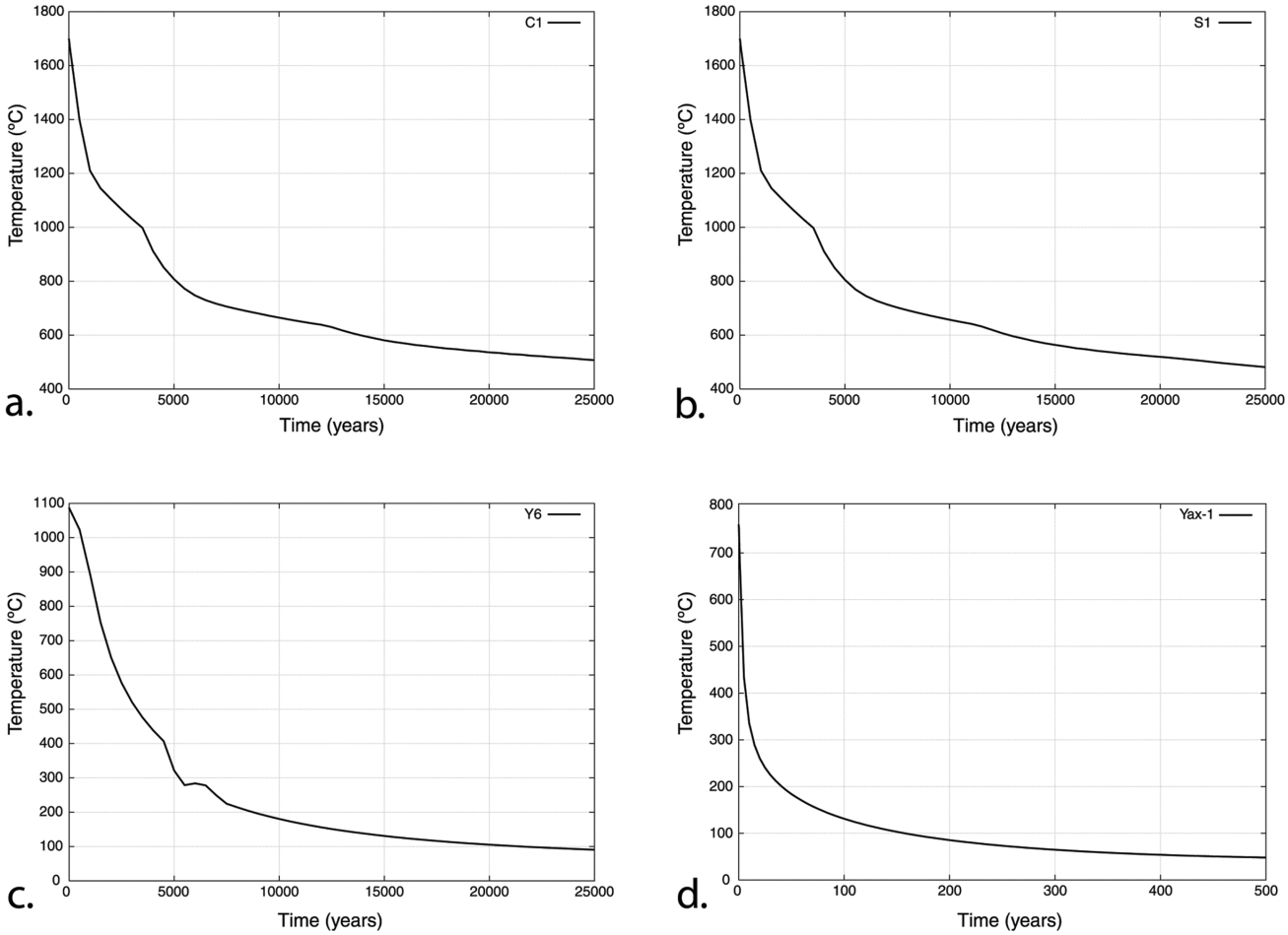

Fig. 4. The temperature history of the melt in the four boreholes within the crater basin: a) C1 (17 km from the center); b) S1 (25 km); c) Y6 (49 km); and d) Yax-1 (62 km). For the first three boreholes, the curves represent the average temperature of the upper 250 m of melt and are not smooth because of the effects of latent heat and convective cooling. The melt in the Yax-1 borehole is below the resolution of the main model and has been modeled separately. The curve for Yax-1 represents the average temperature of the central 8 m of melt.

those in the baseline simulation (k_0 of 10^{-3} darcies). Moreover, this model does not have sufficient water fluxes to remove significant amounts of heat. As a result, the thermal evolution of this model is essentially identical to that of purely conductive one (next section).

Zero-Permeability Case

To further understand the effects of hydrothermal circulation, it is instructive to use a purely conductive model as a control. Conductive cooling of impact craters is well understood and has been modeled by a number of authors (e.g., Onorato et al. 1978; Daubar and Kring 2001; Turtle et al. 2003; Ivanov 2004). HYDROTHERM can be used to model purely conductive heat transport by setting permeability and porosity to near-zero. Figure 6 shows how the Chicxulub crater would have cooled in the complete absence of water. Note that despite "wet" models being generally cooler, vertical heat transport by water can locally increase temperature. This is illustrated by comparing this 2-million-year timestep (Fig. 6d) to that in the higher-permeability model (Fig. 5d), where the 50 and 100 °C contours are closer to the surface in the center of the crater.

System Lifetime

Previously, we defined system lifetime as the time to cool below 90 °C within 1 km of the surface (Abramov and Kring 2004, 2005), with 90 °C representing a doubling of the geothermal temperature at a depth of 1 km in the Sudbury crater model (Abramov and Kring 2004). Although the higher resolution of this model of Chicxulub allows for a measurement closer to the surface, we still use the same definition of system lifetime for easy comparisons with previous models of Sudbury (Abramov and Kring 2004) and Martian craters (Abramov and Kring 2005). Figure 7 illustrates how surface permeability k_0 affects the lifetime, with estimated lifetimes of 1.5 Myr, 1.7 Myr, and 2.3 Myr for permeabilities of 10^{-4}, 10^{-3}, and 10^{-2} darcies, respectively. For comparison, the lifetime of

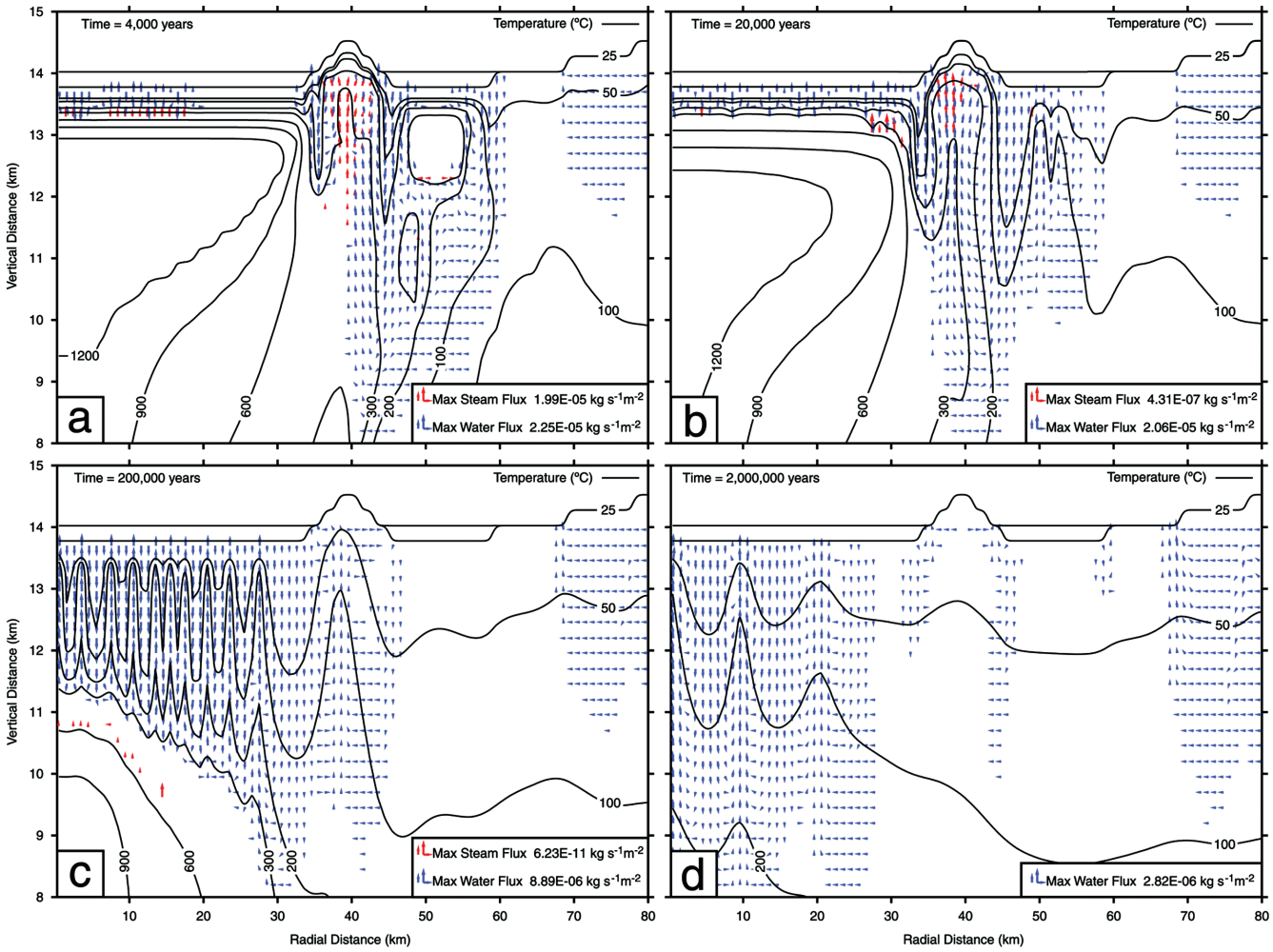

Fig. 5. A higher-permeability simulation of the hydrothermal system at Chicxulub crater. Surface permeability k_0 is 10^{-2} darcies. Black lines are isotherms, labeled in degrees Celsius, and blue and red arrows represent water and steam flux vectors, respectively. The lack of arrows indicates that fluxes are at least two orders of magnitude smaller than the maximum flux. The length of the arrows scales logarithmically with the flux magnitude, and the maximum value of the flux changes with each plot.

the purely conductive case is 1.5 Myr, same as that for a low-permeability system. This type of dependence is similar to that seen for a Martian crater 30 km in diameter (Abramov and Kring 2005), and part of a general pattern observed during the modeling of a wide range of craters. At low permeabilities, little heat is transported by flowing water to the near-surface, resulting in lifetimes similar to the purely conductive case. As permeability increases, significant amounts of heat are delivered to the near-surface, increasing the lifetime of the system, as is seen here. However, as permeability is increased further, this effect is negated by the overall rapid cooling of the system, causing lifetimes to eventually decrease below those for a purely conductive case. The latter effect is not observed in this work due to the lower permeabilities used, but is illustrated in models of other impact craters (Abramov and Kring 2004, 2005).

DISCUSSION

A number of features seen in the model simulations are consistent with those observed at other terrestrial craters. For example, the vigorous circulation in the central region of the crater and beneath the peak ring, seen in Figs. 3 and 5, is consistent with results from drilling into the central uplift of the ~40 km Puchezh-Katunki crater in Russia, which show significant hydrothermal alteration all the way to the bottom of a 5 km borehole (e.g., Naumov 2002).

The model also reveals upward fluid movement in the fault-rich modification zone (Figs. 3 and 5), similar to that described at the 24 km in diameter Haughton crater (Osinski et al. 2001; Osinski et al. 2005). However, it should be noted that water flow does not always follow the normal faults (subtending ~7° clockwise from vertical in the vertically exaggerated Figs. 3 and 5) incorporated into the model, but

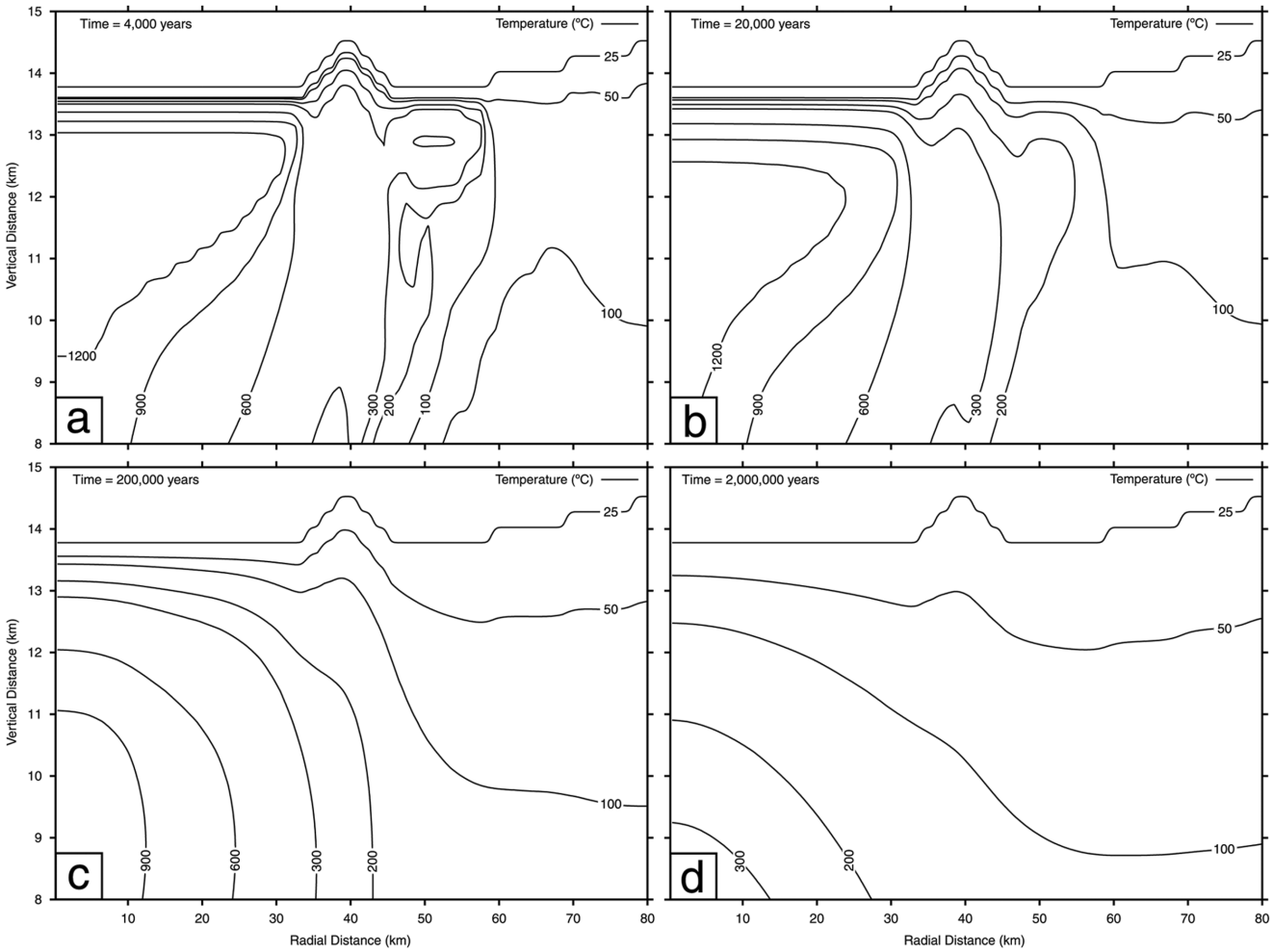

Fig. 6. The thermal evolution of the Chicxulub crater in the absence of water (conductive cooling only). Black lines are isotherms, labeled in degrees Celsius.

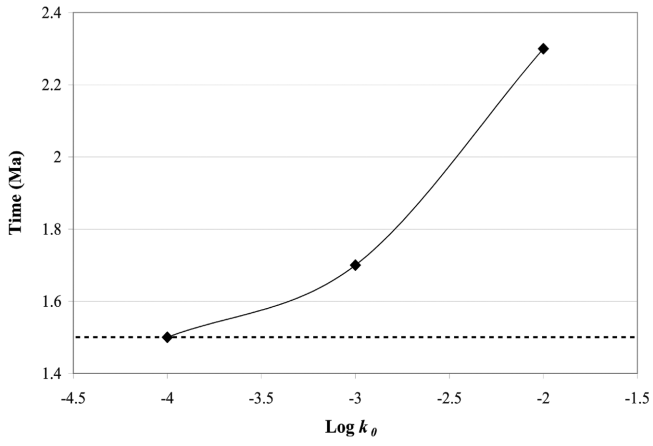

Fig. 7. The effects of permeability on the lifetime of the hydrothermal system at Chicxulub crater. As before, k_0 denotes surface permeability. The dashed line indicates system lifetime in the absence of water flow.

sometimes flows only through the upper (vertical) section of the fault. This is best illustrated by a fault at a radius of ~69 km in Fig. 3d. This behavior may be an artifact of the model, because the faults, which are narrow conduits of extremely high permeability, are difficult to simulate with the model's relatively coarse resolution. More likely, this suggests that upper sections of faults have higher water fluxes because i) the permeability of surrounding rocks is higher at shallower depths, and ii) they are physically closer to the source of the incoming groundwater. We observed similar vertical flow in models of 100 and 180 km diameter craters on early Mars (Abramov and Kring 2005) that did not incorporate faults. This implies that the flow is driven by thermal gradients and topography, and would partly occur even without the localized channels of high permeability provided by faults in the modification zones of craters. However, if faults are present in the modification zone, they will provide conduits for fluid flow and will record alteration assemblages representative of the flow.

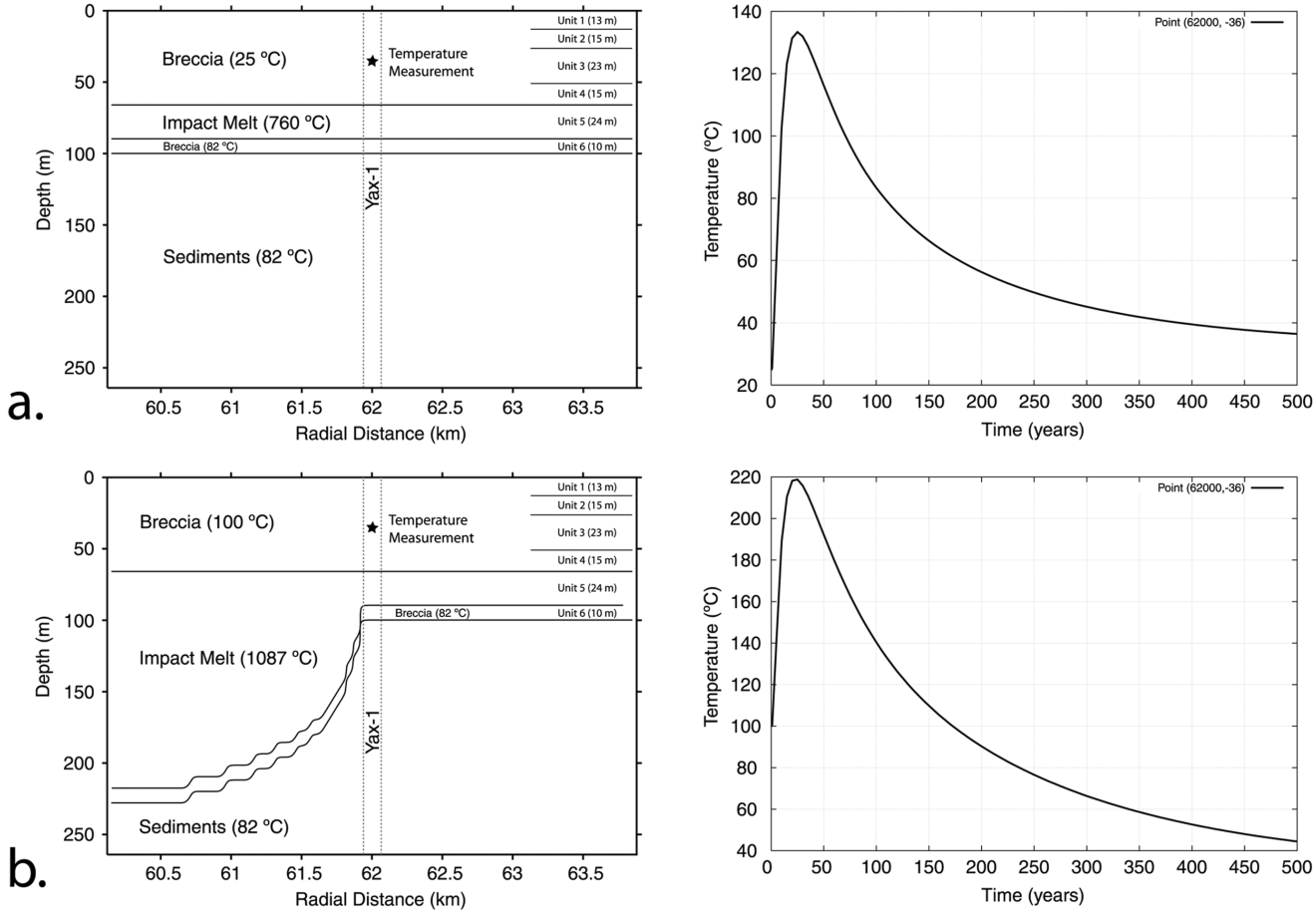

Fig. 8. Temperature profiles in the breccia 30 m above the melt in the Yax-1 borehole, based on a separate thermal conduction model. The left panel shows the initial model setup, and the right panel shows the thermal history at the point marked "Temperature Measurement." a) Most likely scenario; b) "extreme" scenario, with elevated breccia and melt temperatures, as well as a rapidly thickening melt immediately to the left of the borehole.

The model's consistency with observations can also be tested by a comparison to the data derived from analysis of hydrothermally altered samples from the Yax-1 borehole. The model resolution, however, is too coarse for detailed comparison with observations in Yax-1, where the impact-melt rocks are only ~24–34 m thick. We therefore constructed a simple heat conduction cooling model for the local region (Fig. 8a), assuming, as above, that the Yax-1 site was not immediately submerged and remained relatively dry. An earlier model, presented in Zurcher and Kring (2004), only estimated convective heat transport, and predicted that the temperature of the breccia 30 m above the melt would not have been affected by the relatively minor amounts of circulating fluids. In contrast, the present work models conduction, which would have been the dominant form of heat transport. The initial temperatures of the impact melt and overlying breccia were taken directly from a model by Zurcher and Kring (2004), and the temperature below the melt was obtained from the model above for the entire crater. The thickness of the melt unit was conservatively set to 24 m, also following the Zurcher and Kring (2004) model. The regional flow field was not adopted because the purpose of this model was to simply estimate temperatures in the Yax-1 borehole, not to construct a detailed model of hydrothermal circulation in that area of the crater. This would be a challenging task, partly because the Yax-1 breccias were likely unsaturated, and one we leave to future modelers.

The maximum temperature at a point 30 m above the melt, located in the highly altered breccia unit 3, reached 135 °C in the local model. This is significantly less than the temperatures suggested by the alteration mineral assemblages at unit 3, which may have reached or exceeded 300 °C (Zurcher and Kring 2004). Even if we assume higher initial temperatures and a larger volume of nearby melt (Fig. 8b), maximum temperatures in the breccia only reach 220 °C. However, peak conductive temperatures could have been augmented by a localized hydrothermal upwelling and/or horizontal flow, possibly in the form of a rapid, short-lived transient event that was not in equilibrium with the rocks. This is consistent with observations of preferential flow

through localized zones in the Yax-1 core and temperatures of ~270 °C independently derived from fluid inclusions in hydrothermal quartz veins (Lüders et al. 2003; Lüders and Rickers 2004). In addition, the Yax-1 site may have been warmer than indicated in the model, because i) the melt unit could have been up to ~10 m thicker than modeled, and ii) localized melt pools that are seen in the modification zones of craters (Kring 2005), may have increased the temperature of this region, but are not explicitly modeled here.

The shape of the thermal evolution plot of the Yax-1 breccia in the local model (Fig. 8) is also consistent with alteration observed at the Chicxulub crater. The temperature profile shows an initial low-temperature phase, a rapid increase in temperature due to the nearby melt, a brief period of peak temperatures, and a subsequent period of slower cooling, all of which are consistent with the description of Zurcher and Kring (2004) based on observed alteration patterns.

On the scale of the entire impact structure, there is obvious lateral heterogeneity in temperatures at any given timestep. The central regions of the model crater have a much higher initial temperature and remain hot for a far longer period of time, which is consistent the zonation patterns observed during a study of melt samples from the central melt sheet (C1-N10) and two regions of the annular trough (Y6-N19 and Yax-1_863.51) (Zurcher et al. 2005b). A comparison of alteration products from these three boreholes reveals decreasing K-feldspar-quartz to phyllosilicate contents from C1 to Y6 to Yax-1, implying a gradient from higher temperature at C1, to intermediate temperature at Y6, to lower temperature at Yax-1 (Zurcher et al. 2005b). Finally, the duration of hydrothermal activity presented here is consistent with an estimate of "significantly longer than 300 ka" (Rowe et al. 2004), which is derived from the stratigraphic distribution of geochemical anomalies in early Tertiary sediments attributable to hydrothermal plume fallout.

The long duration of the hydrothermal system at Chicxulub, coupled with its large volume, makes it likely that it was colonized by thermophilic (optimal growth temperatures ~50–70 °C) and/or hyperthermophilic (optimal growth temperatures ~70–100 °C) microorganisms. For comparison, the maximum surface area of hydrothermal activity within Chicxulub crater was ~10,000 km^2, while the area of the Yellowstone caldera is smaller, at ~2500 km^2, with continuous hydrothermal activity for only the last ~0.6 Myr (Fournier 1989). Nonetheless, the Yellowstone hydrothermal system is host to a wide variety of microorganisms, and it is therefore likely that Chicxulub was similarly inhabited. In order for these microorganisms to be active, some amount of water flow is needed to bring nutrients and remove waste products. However, the required water flux varies greatly depending on the type of organisms, its chemosynthetic pathway, and the chemical composition of the hydrothermal fluid. Nonetheless, a general habitable zone for (hyper)thermophiles can be estimated from Fig. 3 by examining the rock volume between 50 and 100 °C that has some water flow. As the system evolved, the periphery of the crater cooled fairly quickly, and the habitable zone migrated from the outside inward. Habitable conditions persisted in the central regions of the crater for a far longer time, on the order of hundreds of thousands of years. Thus, a search for prospective biomarkers is most likely to be fruitful in samples from the center of the crater, particularly the polymict breccias overlying the central melt sheet.

To show the variability of hydrothermal systems at craters of similar sizes, it is useful to compare the results of this model of Chicxulub to the model of hydrothermal activity at Sudbury crater (Abramov and Kring 2004). The initial temperature distribution for Sudbury and Chicxulub is not significantly different. The Chicxulub model has a larger melt sheet, with a central thickness of 3.5 km, versus 2.5 km for Sudbury (e.g., Grieve 1994; Pope et al. 2004). However, this is partly compensated for by the fact the outer regions of the crater are cooler than those at Sudbury. The melt temperature in the annular trough is set to 1087 °C, versus 1700 °C. Comparing the baseline model (surface permeability of 10^{-3} darcies) in this paper to the Sudbury model of analogous permeability, we note that the fluxes are generally higher for Sudbury, partly due to the 1.5 km of permeable breccias above the melt. The thickness of breccias at Sudbury is greater than that estimated for Chicxulub based on drill cores and geophysical data, which affects both hydrothermal circulation and thermal evolution. The Sudbury model is cooling more slowly than that of Chicxulub, partly due to the lower thermal conductivity used, and partly due to the insulating effects of the additional breccia overburden. For the same breccia thickness (500 m), the lifetime of the 10^{-3} darcy model in this paper (1.7 Myr) is slightly less than the lifetime in the Sudbury model of the same permeability (1.9 Myr). However, for the higher-permeability model (surface permeability of 10^{-2} darcies), the system lifetime is significantly higher for Chicxulub than for Sudbury: 2.3 Myr versus 1.1 Myr. This is mainly due to system dynamics; towards the end of the system there are many central convection cells in the Sudbury model, but for Chicxulub there are only a couple, and a strong central upwelling concentrates heat in the center of the crater. The higher initial temperatures in the center of the Chicxulub crater also contribute to longer lifetimes.

Some of the differences are an artifact of modeling. Specifically, an increase in the spatial resolution of simulations appears to increase the number of convection cells above the central uplift in the later stages of cooling, particularly for the higher-permeability case. The number of convection cells is also a function of permeability, with a higher number of cells in higher-permeability models.

An important process affecting hydrothermal systems is self-sealing as a result of alteration and mineral deposition,

which has been observed in drillcores from the Yellowstone geothermal system (Keith et al. 1978). Although it is possible to incorporate this process into the model in an approximate way, for example, as a linear or exponential decrease with time, this approach may not adequately represent physical reality. A recent study by Dobson et al. (2003) of self-sealing at the Yellowstone geothermal system suggests that, although it can decrease the permeability and porosity of the rock matrix, it focuses fluid flow along fractures, where multiple episodes of fluid flow and self-sealing have occurred. Because impact craters have a high fracture density, permeability of an impact crater must be dominated by macroscopic fractures (e.g., Mayr et al. 2005), and therefore fluid flow is more likely to occur in cyclical episodes described by Dobson et al. (2003) rather than decrease smoothly with time. A typical cycle begins with an explosive release of fluid overpressure, which forms transient, high-flow conduits, and the subsequent fluid flow results in mineral precipitation and eventual self-sealing, leading to another cycle of the process (Dobson et al. 2003). The simulations presented in this paper thus represent an average fluid flow.

CONCLUSIONS

The modeling results presented in this work suggest the following sequence of hydrothermal activity at Chicxulub crater: Shortly after the impact, a partial flooding of the deepest portions of the crater infiltrated the permeable breccias overlying the melt, resulting in rapid steam emission for ~2000 yr, followed by the circulation of water through these breccias. The melt in the annular trough crystallized in less than ~600 yr, but the region remained hot and impermeable for thousands of years thereafter. Initial hydrothermal activity was not limited to breccias, however, as convection cells quickly formed at the edges of both the central melt sheet and the melt in the annular trough, with some water flow underneath the latter. In addition, faults in the crater's modification zone provided conduits for an upward flow of water. As the system evolved, flux magnitudes generally decreased and hydrothermal activity moved from the outside of the crater inward. Temperature contours were vertically deflected by the upward flow of warmer water and downward flow of colder water, and long-lived upwellings, such as the one beneath the peak ring, were established. As the impact melt cooled, it gradually became brittle and fractured, becoming permeable to water. The melt in the annular trough became permeable quickly, in ~5000 yr, while it took the central melt sheet several hundred thousand years to become fully permeable. In the later stages of the hydrothermal system, numerous convection cells formed above the central uplift, resulting in significant circulation of water and steam through the solidified central melt sheet. In the final stages of activity, warm temperatures were maintained in the center of the crater by a single central upwelling, which delivered heat from the deep interior to the near-surface.

The temperatures and fluxes observed in the model are consistent with alteration patterns observed in the samples from Chicxulub crater. The central regions of the model crater have a much higher initial temperature and remain hot for a far longer period of time, which is consistent the zonation patterns suggesting a gradient from higher temperatures at the center to lower temperatures at the periphery. A separate thermal submodel put together for the Yax-1 borehole shows an initial low-temperature phase in the polymict breccia, a rapid increase in temperature due to the nearby melt, a brief period of peak temperatures, and a subsequent period of slower cooling, which is consistent with mineralogical signatures observed in the samples. Although a maximum temperature of just 220 °C was reached in this test, higher temperatures could have been reached through a localized hydrothermal upwelling, horizontal flow, permeability variations, and other mechanisms.

The lifetime of the hydrothermal system ranges from 1.5 to 2.3 Myr depending on assumed permeability. To first order, these values agree with an estimate derived from geochemical anomalies in the early Tertiary sediments. These lifetimes are longer than those obtained from a model of a similarly sized Sudbury crater, partly due to a larger central melt sheet at Chicxulub (central thickness of 3.5 km, versus 2.5 km for Sudbury). The relatively long duration of hydrothermal activity presented here is explained by several factors. First, permeability decreases exponentially with depth and large parts of the crater are impermeable due to high temperatures, relegating most hydrothermal cooling to near-surface regions while the bulk of the crater is dominated by conduction. Second, significant amounts of heat are delivered to the near-surface by hydrothermal upwellings, increasing the lifetime of the system. Finally, the permeability range used here is too low to overcome this effect and allow a rapid convective cooling of the crater.

The long duration of the hydrothermal system at Chicxulub provided ample time for colonization by thermophiles and/or hyperthermophiles. The habitable zone for these microorganisms migrated from the outside inward as the crater cooled. Because habitable conditions persisted in the central regions of the crater for a far longer time than the periphery, a search for prospective biomarkers is most likely to be fruitful in samples from that region.

Acknowledgments–This work was supported by NASA grant NAG512691 from the Mars Fundamental Research Program. We thank Lukas Zurcher for numerous helpful discussions and comments regarding this manuscript. We also thank Boris Ivanov for providing the Chicxulub temperature distribution used in this work. We gratefully acknowledge the use of supercomputer resources at the High Performance Computing

facility of the University of Arizona. Last but not least, we express thanks to Argo Jõeleht and Gordon "Oz" Osinski for their detailed and insightful reviews of this manuscript. LPI Contribution #1336.

Editorial Handling—Dr. Elisabetta Pierazzo

REFERENCES

Abramov O. and Kring D. A. 2004. Numerical modeling of an impact-induced hydrothermal system at the Sudbury crater. *Journal of Geophysical Research* 109, doi:10.1029/2003JE002213.

Abramov O. and Kring D. A. 2005. Impact-induced hydrothermal activity on early Mars. *Journal of Geophysical Research* 110, doi:10.1029/2005JE002453.

Ahrens T. J. and O'Keefe J. D. 1972. Shock melting and vaporization of lunar rocks and minerals. *The Moon* 4:214–249.

Ames D. E., Watkinson D. H., and Parrish R. R. 1998. Dating of a regional hydrothermal system induced by the 1850 Ma Sudbury impact event. *Geology* 26:447–450.

Ames D. E., Kjarsgaard I. M., Pope K. O., Dressler B., and Pilkington M. 2004. Secondary alteration of the impactite and mineralization in the basal Tertiary sequence, Yaxcopoil-1, Chicxulub impact crater, Mexico. *Meteoritics & Planetary Science* 39:1145–1167.

Ariskin A. A., Deutsch A., and Ostermann M. 1999. The Sudbury "igneous" complex: Simulating phase equilibria and in situ differentiation for two proposed parental magmas. In *Large meteorite impacts and planetary evolution II,* edited by Dressler B. O. and Sharpton V. L. GSA Special Paper #339. Boulder, Colorado: Geological Society of America. pp. 337–387.

Barron E. J. 1983. A warm, equable Cretaceous: The nature of the problem. *Earth Science Review* 19:305–338.

Bell C., Morgan J. V., Hampson G. J., and Trudgill B. 2004. Stratigraphic and sedimentological observations from seismic data across the Chicxulub impact basin. *Meteoritics & Planetary Science* 39:1089–1098.

Binder A. B. and Lange M. A. 1980. On the thermal history, thermal state, and related tectonism of a moon of fission origin. *Journal of Geophysical Research* 85:3194–3208.

Carstens H. 1975. Thermal history of impact melt rocks in the Fennoscandian Shield. *Contributions to Mineralogy and Petrology* 50:145–155.

Christeson G. L., Nakamura Y., Buffler R. T., Morgan J., and Warner M. 2001. Deep crustal structure of the Chicxulub impact crater. *Journal of Geophysical Research* 106:21,751–21,769.

Clifford M. 1993. A model for the hydrologic and climatic behavior of water on Mars. *Journal of Geophysical Research* 98:10,973–11,016.

Clark S. P. 1966. Thermal conductivity. In *Handbook of physical constants,* edited by Clark S. P. Memoir #97. New York: Geological Society of America. pp. 459–482.

Cohen B. A., Swindle T. D., and Kring D. A. 2000. Support for the lunar cataclysm hypothesis from lunar meteorite impact melt ages. *Science* 290:1754–1756.

Collins G. S., Melosh H. J., Morgan J. V., and Warner M. R. 2002. Hydrocode simulations of Chicxulub crater collapse and peak-ring formation. *Icarus* 157:24–33.

Daubar I. J. and Kring D. A. 2001. Impact-induced hydrothermal systems: Heat sources and lifetimes (abstract #1727). 32nd Lunar and Planetary Science Conference. CD-ROM.

Dobson P. F., Kneafsey T. J., Hulen J., and Simmons A. 2003. Porosity, permeability, and fluid flow in the Yellowstone geothermal system, Wyoming. *Journal of Volcanology and Geothermal Research* 123:313–324.

Dressler B. O., Sharpton V. L., Morgan J., Buffler R., Moran D., Smit J., Stöffler D., and Urrutia J. 2003. Investigating a 65-Ma-old smoking gun: Deep drilling of the Chicxulub impact structure. *Eos* 84:125–130.

Ebbing J., Janle P., Koulouris J., and Milkereit B. 2001. 3D gravity modelling of the Chicxulub impact structure. *Planetary and Space Science* 49:599–609.

El Goresy A. 1965. Baddeleyite and its significance in impact glasses. *Journal of Geophysical Research* 70:3453–3456.

Englehardt von W., Arndt J., Fecker B., and Pankau H. G. 1995. Suevite breccia from the Ries crater, Germany: Origin, cooling history and devitrification of impact glasses. *Meteoritics* 30:279–293.

Farrow C. E. G. and Watkinson D. H. 1992. Alteration and the role of fluids in Ni, Cu and platinum-group element deposition, Sudbury Igneous Complex contact, Onaping-Levack area, Ontario. *Mineralogy and Petrology* 46:611–619.

Fournier R. O. 1989. Geochemistry and dynamics of the Yellowstone National Park hydrothermal system. *Annual Review of Earth and Planetary Sciences* 17:13–53.

Fournier R. O. 1991. The transition from hydrostatic to greater than hydrostatic fluid pressure in presently active continental hydrothermal systems in crystalline rock. *Geophysical Research Letters* 18:955–958.

Frakes L. A. 1979. *Climates through geologic time*. Amsterdam: Elsevier Scientific Publication Company. 310 p.

Grieve R. A. F. 1994. An impact model of the Sudbury structure. Proceedings of Sudbury-Noril'sk Symposium. Ontario Geological Survey, Special Volume 5. pp. 119–132.

Grieve R. A. F. and Pesonen L. J. 1992. The terrestrial impact cratering record. *Tectonophysics* 216:1–30.

Grieve R. A. F., Dence M. R., and Robertson P. B. 1977. Cratering processes: As interpreted from the occurrence of impact melts. In *Impact and explosion cratering,* edited by Roddy D. J., Pepin R. O., and Merrill R. B. New York: Pergamon Press. pp. 791–814.

Goto K., Tada R., Tajika E., Bralower T. J., Hasegawa T., and Matsui T. 2004. Evidence for ocean water invasion into the Chicxulub crater at the Cretaceous/Tertiary boundary. *Meteoritics & Planetary Science* 39:1233–1247.

Gulick V. C. 2001. Some ground water considerations regarding the formation of small Martian gullies (abstract #2193). 32nd Lunar and Planetary Science Conference. CD-ROM.

Hayba D. O. and Ingebritsen S. E. 1994. The computer model HYDROTHERM, a three-dimensional finite-difference model to simulate ground-water flow and heat transport in the temperature range of 0 to 1,200 degrees Celsius. U.S. Geological Survey Water-Resources Investigations Report 94-4045. Reston, Virginia: U.S. Geological Survey. 85 p.

Hayba D. O. and Ingebritsen S. E. 1997. Multiphase groundwater flow near cooling plutons. *Journal of Geophysical Research* 102: 12,235–12,252.

Hecht L., Wittmann A., Schmitt R. T., and Stöffler D. 2004. Composition of impact melt particles and the effects of post-impact alteration in suevitic rocks at the Yaxcopoil-1 drill core, Chicxulub crater, Mexico. *Meteoritics & Planetary Science* 39: 1169–1186.

Hildebrand A. R., Penfield G. T., Kring D. A., Pilkington M., Camargo A. Z., Jacobson S. B., and Boynton W. V. 1991. A possible Cretaceous-Tertiary boundary impact crater on the Yucatán Peninsula, Mexico. *Geology* 19:867–871.

Hörz F. 1965. Untersuchungen an Riesgläsern. *Beiträge zur Mineralogie und Petrologie* 11:621–661.

Huber B. T., Hodell D. A., and Hamilton C. P. 1995. Middle-late Cretaceous climate of the southern high latitudes: Stable isotopic evidence for minimal equator-to-pole thermal gradients. *Geological Society of America Bulletin* 107:1164–1191.

Ivanov B. A. 2004. Heating of the lithosphere during meteorite cratering. *Solar System Research* 38:266–278.

Jaeger J. C. 1968. Cooling and solidification of igneous rocks in basalts. In *The Poldervaart treatise on rocks of basaltic composition,* edited by Hess H. H. and Poldervaart A. New York: John Wiley. pp. 503–535.

Keith T. E. C., White D. E., and Beeson M. H. 1978. Hydrothermal alteration and self-sealing in Y-7 and Y-8 drill holes in northern part of Upper Geyser Basin, Yellowstone National Park, Wyoming. Professional Paper 1054-A. Denver, Colorado: U.S. Geological Survey. 26 p.

Kettrup B. and Deutsch A. 2003. Geochemical variability of the Yucatán basement: Constraints from crystalline clasts in Chicxulub impactites. *Meteoritics & Planetary Science* 38: 1079–1092.

Kolodny Y. and Raab M. 1988. Oxygen isotopes in phosphatic fish remains from Israel: Paleothermometry of tropical Cretaceous and Tertiary shelf waters. *Palaeogeography, Palaeoclimatology, Palaeoecology* 64:59–67.

Kring D. A. 1995. The dimensions of the Chicxulub impact crater and impact melt sheet. *Journal of Geophysical Research* 100:16,979–16,986.

Kring D. A. 2000. Impact events and their effect on the origin, evolution, and distribution of life. *GSA Today* 10:1–7.

Kring D. A. 2005. Hypervelocity collisions into continental crust composed of sediments and an underlying crystalline basement: Comparing the Ries (~24 km) and Chicxulub (~180 km) impact craters. *Chemie der Erde* 65:1–46.

Kring D. A. Forthcoming. The Chicxulub impact event and its environmental consequences at the K/T boundary. *Paleogeography, Paleoclimatology, Paleoecology.*

Kring D. A. and Boynton W. V. 1992. The petrogenesis of an augite-bearing melt rock in the Chicxulub structure and its relationship to K/T impact spherules in Haiti. *Nature* 358:141–144.

Kring D. A. and Cohen B. A. 2002. Cataclysmic bombardment throughout the inner solar system 3.9–4.0 Ga. *Journal of Geophysical Research* 107, doi:10.1029/2001JE001529.

Kring D. A., Hildebrand A. R., and Boynton W. V. 1991. The petrology of an andesitic melt rock and a polymict breccia from the interior of the Chicxulub structure, Yucatán, Mexico (abstract). 22nd Lunar and Planetary Science Conference. pp. 755–756.

Kring D. A., Zurcher L., Hörz F., and Urrutia Fucugauchi J. 2004. Impact lithologies and their emplacement in the Chicxulub impact crater: Initial results from the Chicxulub Scientific Drilling Project, Yaxcopoil, Mexico. *Meteoritics & Planetary Science* 39:879–897.

Lüders V. and Rickers K. 2004. Fluid inclusion evidence for impact-related hydrothermal fluid and hydrocarbon migration in Cretaceous sediments of the ICDP-Chicxulub drill core Yax-1. *Meteoritics & Planetary Science* 39:1187–1197.

Lüders V., Horsfield B., Kenkmann T., Mingram B., and Wittmann A. 2003. Hydrocarbons and aqueous fluids in Cretaceous sediments of the ICDP-Chicxulub drill core Yax-1 (abstract #1378). 34th Lunar and Planetary Science Conference. CD-ROM.

Manning C. E. and Ingebritsen S. E. 1999. Permeability of the continental crust: Implications of geothermal data and metamorphic systems. *Reviews of Geophysics* 37:127–150.

Mayr S., Burkhardt H., Popov Yu., Romushkevich R., and Bayuk I. 2005. Geothermal and petrophysical investigations within the Chicxulub Scientific Drilling Project—Physical properties of rocks in the borehole Yax-1 (abstract). Integrated Ocean Drilling Program/International Continental Drilling Program Joint Meeting. CD-ROM.

Mojzsis S. J. and Harrison T. M. 2000. Vestiges of a beginning: Clues to the emergent biosphere recorded in the oldest known sedimentary rocks. *GSA Today* 10:1–6.

Morgan J., Warner M., Brittan J., Buffler R., Camargo A., Christeson G., Dentons P., Hildebrand A., Hobbs R., MacIntyre H., Mackenzie G., Maguires P., Marin L., Nakamura Y., Pilkington M., Sharpton V., and Snyders D. 1997. Size and morphology of the Chicxulub impact crater. *Nature* 390: 472–476.

Morgan J. V., Warner M. R., Collins G. S., Melosh H. J., and Christeson G. L. 2000. Peak ring formation in large impact craters: Geophysical constraints from Chicxulub. *Earth and Planetary Science Letters* 183:347–354.

Morgan J. V., Christeson G. L., and Zelt C. A. 2002. Testing the resolution of a 3D velocity tomogram across the Chicxulub crater. *Tectonophysics* 355:215–226.

Naumov M. V. 2002. Impact-generated hydrothermal systems: Data from Popigai, Kara, and Puchezh-Katunki impact structures. In *Impacts in Precambrian shields,* edited by Plado J. and Pesonen L. J. New York: Springer. pp. 117–171.

Nordyke M. D. 1964. Cratering experience with chemical and nuclear explosives. Proceedings, Third Plowshare Symposium-Engineering with Nuclear Explosives. U.S. Atomic Energy Commission Report TID-7695. pp. 51–73.

O'Keefe J. D. and Ahrens T. J. 1977. Impact-induced energy partitioning, melting, and vaporization on terrestrial planets. Proceedings, 8th Lunar Science Conference. pp. 3357–3374.

Onorato P. I. K., Uhlmann D. R., and Simonds C. H. 1978. The thermal history of the Manicouagan impact melt sheet, Quebec. *Journal of Geophysical Research* 83:2789–2798.

Osinski G. R., Spray J. G., and Lee P. 2001. Impact-induced hydrothermal activity in the Haughton impact structure, Canada: Generation of a transient, warm, wet oasis. *Meteoritics & Planetary Science* 36:731–745.

Osinski G. R., Grieve R. A. F., and Spray J. G. 2004. The nature of the groundmass of surficial suevite from the Ries impact structure, Germany, and constraints on its origin. *Meteoritics & Planetary Science* 39:1655–1683.

Osinski G. R., Lee P., Parnell J., Spray J. G, and Baron M. 2005. A case study of impact-induced hydrothermal activity: The Haughton impact structure, Devon Island, Canadian High Arctic. *Meteoritics & Planetary Science* 40:1859–1877.

Pace N. R. 1997. A molecular view of microbial diversity and the biosphere. *Science* 276:734–740.

Phinney W. C. and Simonds C. H. 1977. Dynamical implications of the petrology and distribution of impact melt rocks. In *Impact and explosion cratering,* edited by Roddy D. J., Pepin R. O., and Merrill R. B. New York: Pergamon Press. pp. 771–790.

Pierazzo E., Kring D. A., and Melosh H. J. 1998. Hydrocode simulation of the Chicxulub impact event and the production of climatically active gases. *Journal of Geophysical Research* 103: 28,607–28,626.

Pike R. 1977. Size dependence in the shape of fresh impact craters on the Moon. In *Impact and explosion cratering,* edited by Roddy D. J., Pepin R. O., and Merrill R. B. New York: Pergamon Press. pp. 489–509.

Pilkington M., Hildebrand A. R., and Ortiz-Aleman C. 1994. Gravity and magnetic field modeling and structure of the Chicxulub Crater, Mexico. *Journal of Geophysical Research* 99:13,147–13,162.

Pope K. O., Kieffer S. W., and Ames D. E. 2004. Empirical and

theoretical comparisons of the Chicxulub and Sudbury impact structures. *Meteoritics & Planetary Science* 39:97–116.

Popov Yu., Romushkevich R., Bayuk I., Korobkov D., Mayr S., Burkhardt H., and Wilhelm H. 2004. Physical properties of rocks from the upper part of the Yaxcopoil-1 drillhole, Chicxulub crater. *Meteoritics & Planetary Science* 39:799–812.

Prevec S. A. and Cawthorn R. G. 2002. Thermal evolution and interaction between impact melt sheet and footwall: A genetic model for the contact sublayer of the Sudbury Igneous Complex, Canada. *Journal of Geophysical Research* 107, doi:10.1029/2001JB000525.

Rathbun J. A. and Squyres S. W. 2002. Hydrothermal systems associated with Martian impact craters. *Icarus* 157:362–372.

Robertson P. B. and Grieve R. A. F. 1977. Shock attenuation at terrestrial impact structures. In *Impact and explosion cratering,* edited by Roddy D. J., Pepin R. O., and Merrill R. B. New York: Pergamon Press. pp. 687–702.

Rowe A. J., Wilkinson J. J., Coles B. J., and Morgan J. V. 2004. Chicxulub: Testing for post-impact hydrothermal input into the Tertiary ocean. *Meteoritics & Planetary Science* 39:1223–1231.

Ryder G. 1990. Lunar samples, lunar accretion, and the early bombardment of the Moon. *Eos* 71:322–323.

Ryder G. 2000. Ancient intense impacting: A positive effect on the origin of life (abstract #B22B-01). *Eos* 81, 2000 AGU Spring Meeting.

Schuraytz B. C., Sharpton V. L., and Marin L. E. 1994. Petrology of impact-melt rocks at the Chicxulub multiring basin, Yucatán, Mexico. *Geology* 22:868–872.

Sharpton V. L., Dalrymple G. D., Marin L. E., Ryder G., Schuraytz B. C., and Urruita-Fucugauchi J. 1992. New links between the Chicxulub impact structure and the Cretaceous/Tertiary boundary. *Nature* 359:819–820.

Sharpton V. L., Marín L. E., Carney J. L., Lee S., Ryder G., Schuraytz B. C., Sikora P., and Spudis P. D. 1996. A model of the Chicxulub impact basin based on evaluation of geophysical data, well logs, and drill core samples. In *The Cretaceous-Tertiary event and other catastrophes in Earth history,* edited by Ryder G., Fastovsky D., and Gartner S. GSA Special Paper #307. Boulder, Colorado: Geological Society of America. pp. 55–74.

Simonds C. H., Warner J. L., Phinney W. C., and McGee P. E. 1976. Thermal model for impact breccia lithification: Manicouagan and the Moon. Proceedings, 7th Lunar Science Conference. pp. 2509–2528.

Stöffler D., Artemieva N. A., Ivanov B. A., Hecht L., Kenkmann T., Schmitt R. T., Tagle R. A., and Wittmann A. 2004. Origin and emplacement of the impact formations at Chicxulub, Mexico, as revealed by the ICDP deep drilling at Yaxcopoil-1 and by numerical modeling. *Meteoritics & Planetary Science* 39:1035–1067.

Tera F., Papanastassiou D. A., and Wasserburg G. J. 1974. Isotopic evidence for a terminal lunar cataclysm. *Earth and Planetary Science Letters* 22:1–21.

Thorsos I. E., Newsom H. E., and Davies A. D. 2001. Availability of heat to drive hydrothermal systems in large Martian impact craters (abstract #2011). 32nd Lunar and Planetary Science Conference. CD-ROM.

Turner G., Cadogan P. H., and Yonge C. J. 1973. Argon selenochronology. Proceedings, 4th Lunar Science Conference. pp. 1889–1914.

Turtle E. P., Pierazzo E., and O'Brien D. P. 2003. Numerical modeling of impact heating of the Vredefort impact structure. *Meteoritics & Planetary Science* 38:293–303.

Upchurch G. R. and Wolfe J. A. 1987. Mid-Cretaceous to Early Tertiary vegetation and climate: Evidence from fossil leaves and wood. In *The origins of angiosperms and their biological consequences,* edited by Friis E. M., Chaloner W. G., and Crane P. R. Cambridge: Cambridge University Press. pp. 75–105.

Versh E., Kirsimäe K., Jõeleht A., and Plado J. 2005. Cooling of the Kärdla impact crater: I. The mineral paragenetic sequence observation. *Meteoritics & Planetary Science* 40:3–19.

Warren P. H., Claeys P., and Cedillo-Pardo E. 1996. Mega-impact melt petrology (Chicxulub, Sudbury, and the Moon): Effects of scale and other factors on potential for fractional crystallization and development of cumulates. In *The Cretaceous-Tertiary event and other catastrophes in Earth history,* edited by Ryder G., Fastovsky D., and Gartner S. GSA Special Paper #307. Boulder, Colorado: Geological Society of America. pp. 105–124.

Wilhelm H., Heidinger P., Šafanda J., Èermak V., Burkhardt H., and Popov Y. 2004. High resolution temperature measurements in the borehole Yaxcopoil 1, Mexico. *Meteoritics & Planetary Science* 39:813–819.

Wittmann A., Kenkmann T., Schmitt R. T., Hecht L., and Stöffler D. 2004. Impact-related dike breccia lithologies in the ICDP drill core Yaxcopoil-1, Chicxulub impact structure, Mexico. *Meteoritics & Planetary Science* 39:931–954.

Wittmann A., Kenkmann T., Schmitt R. T., Hecht L., and Stöffler D. 2005. Shock metamorphism and thermal annealing of zircon in the ICDP-Chicxulub drill core Yaxcopoil-1 (abstract). Integrated Ocean Drilling Program/International Continental Drilling Program Joint Meeting. CD-ROM.

Zurcher L. and Kring D. A. 2004. Hydrothermal alteration in the Yaxcopoil-1 borehole, Chicxulub impact structure, Mexico. *Meteoritics & Planetary Science* 39:1199–1222.

Zurcher L., Kring D. A., Dettman D., and Rollog M. 2005a. Stable isotope record of post-impact fluid activity in the Yaxcopoil-1 borehole, Chicxulub impact structure, Mexico. In *Large meteorite impacts and planetary evolution III,* edited by Kenkmann T., Hörz F., and Deutsch A. GSA Special Paper #384. Boulder, Colorado: Geological Society of America. pp. 323–338.

Zurcher L., Lounejeva-Baturina E., and Kring D. A. 2005b. Preliminary analysis of relative abundances of hydrothermal alteration products in the C1-N10, Y6-N19, and Yax-1_863.51 impact melt samples, Chicxulub structure, Mexico (abstract #1983). 36th Lunar and Planetary Science Conference. CD-ROM.